OPTIMIZATION OF ITER WITH ITER-89P SCALING

J. JOHNER

October 1991

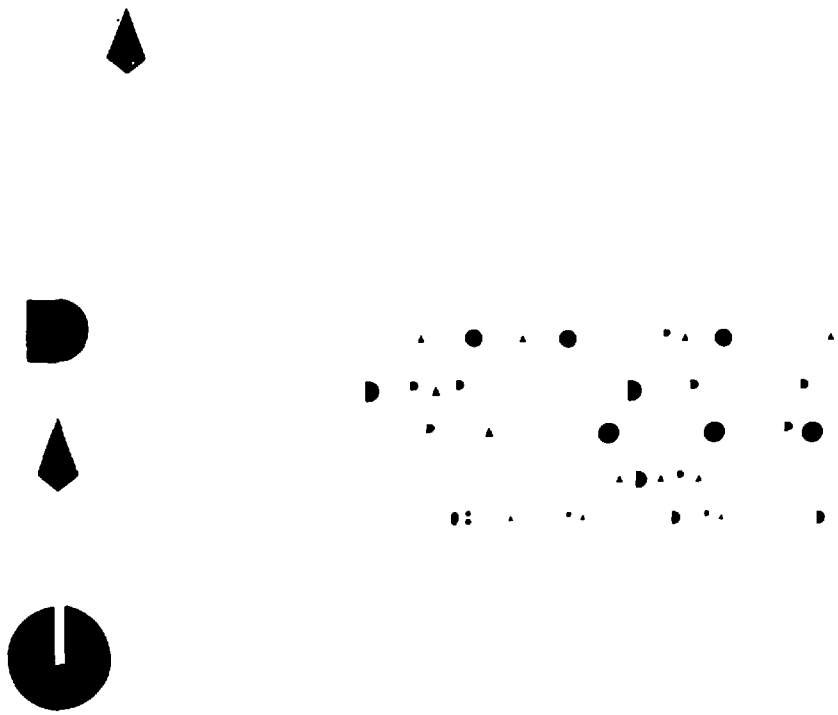

OPTIMIZATION OF ITER
WITH ITER-89P SCALING

J. JOHNER

ASSOCIATION EURATOM-CEA SUR LA FUSION
Département de Recherches sur la Fusion Contrôlée
Centre d'Etudes Nucléaires de Cadarache
13108 SAINT-PAUL-LEZ-DURANCE CEDEX (FRANCE)

ABSTRACT

Ignition in the ITER baseline machine (a=2.15 m, R=6 m, B_t=4.85 T, I_p=22 MA), is studied in the frame of a 1/2-D model using the ITER-89P scaling of the energy confinement time.

The required value of the enhancement factor f_L with respect to the L-mode, allowing ignition with a total fusion power of 1100 MW, is found to be 1.9 at an optimum operating temperature of 11 keV. A sensitivity analysis shows that the critical f_L=2 value can be exceeded with relatively small changes in the physical assumptions. It is concluded that the safety margin is not sufficient for this project.

Optimization of a thermonuclear plasma in a tokamak is then performed with constraints of given maximum magnetic field B_{tmax} in the superconducting windings, given distance d_{BS} between the plasma and the maximum magnetic field point, imposed safety factor q_ψ at the plasma edge, and given averaged neutron flux Γ_n at the plasma surface. It is shown that the minimum enhancement factor f_L with respect to the L-mode, allowing ignition at a given value of the total fusion power P_{fus}, is only a function of the torus aspect ratio A.

Taking the ITER reference values for the above constraints (i.e. $B_{tmax} \simeq 11$ T, $d_{BS} \simeq 1.1$ m, $q_\psi \simeq 3$, $\Gamma_n \simeq 1$ MW/m²), it is found that the required value of f_L is practically independent of the aspect ratio (very broad minimum in A) but can be sensibly improved by increasing the total fusion power P_{fus}. With P_{fus}=1700 MW, a reasonable safety margin ($f_L \simeq 1.5$) is obtained. With such a power, the machine corresponding to an aspect ratio A=4, which would be favourable for the technology phase, is found to have $a \simeq 2.22$ m, $R \simeq 8.87$ m, $B_t \simeq 6.66$ T, $I_p \simeq 20.2$ MA.

Analytical expressions of the conditions resulting from the above optimization are also derived for an arbitrary monomial scaling of the energy confinement time, and shown to give excellent agreement with the numerical results.

1. INTRODUCTION

The ITER baseline machine [1] is obtained by an optimization procedure where the following constraints are retained:

- imposed maximum magnetic field in the superconducting windings ($B_{tmax} \simeq 11$ T),
- given value of the blanket plus shield width ($d_{BS} \simeq 1$ m),
- given value of the safety factor at the magnetic surface enclosing 95% of the poloidal flux ($q_\psi \simeq 3$),
- given value of the averaged neutron load on the first wall (1 MW/m²),
- given value of the enhancement factor with respect to the ITER-89P L-mode scaling of the energy confinement time (f_L=2),
- given density-averaged temperature of operation ([T]=10 keV),
- given inductive burn time t_{burn}=400 s for an internal inductance l_i=0.65.

With the above constraints and the usual ITER assumptions concerning the plasma composition, profiles, and shape of the poloidal section, it is shown that the machine is completely determined, giving A=2.79, a=2.15 m, B_t=4.85 T, I_p=22 MA, where a is the horizontal minor radius, I_p the total plasma current, and B_t the magnetic field on the magnetic axis.

In the present study, a somewhat different optimization is performed in order to assess the sensitivity of the confinement requirements with respect to the design assumptions. In the optimization scheme, the above first four constraints are retained together with the value of the total fusion power P_{fus}. The enhancement factor required for ignition in these conditions appears to be only a function of the operating temperature and of the aspect ratio. It will be shown that this value of f_L exhibits a minimum with respect to the latter two parameters. Choosing these optimum conditions completely determines the machine parameters as well as the plasma operating point.

In section 2, we recall the main features of the 1/2-D stationary model implemented in the present version of the HELIOS code.

In section 3, we give the approximate analytical conditions obtained with the ITER-89P scaling, for the possibility of ignition with an imposed value of the total fusion power or of the averaged neutron flux at the plasma surface. We also derive the analytical criterion for ignition when both the above constraints are assumed as well as the constraint on the value of the maximum magnetic field inside the superconducting windings. The correspondg conditions for a general monomial scaling are given in Appendix D.

In section 4, ignition in ITER with the reference parameters and assumptions is studied. A sensitivity analysis is also performed by varying different parameters around the reference values.

In section 5, we show the existence of optimum values of the operating temperature and aspect ratio for ignition with given B_{tmax}, d_{BS}, q_ψ, Γ_n, and P_{fus}. The corresponding minimum value of the L-mode enhancement factor is calculated as a function of the total fusion power. The machines corresponding to P_{fus}=1100, 1700, 2200, and 3500 MW are described. A machine with P_{fus}=1700 MW and a larger aspect ratio (A=4) is also discussed in some details.

SI units are used except for the temperature which is always expressed in keV ($k=1.6022\times10^{-16}$ J/keV).

2. THE MODEL

In this section, we describe the model implemented in the present version of the HELIOS code. Improvements with respect to the previous version [2,3] are the following:

- modelisation of the outer magnetic surface poloidal section allowing the description of plasmas with an inner/outer dissymetric separatrix with two X-points,

- arbitrary ratio T_e/T_i (radially constant) introduced in all the terms of the thermal equilibrium equation,

- introduction of the Sadler-Van Belle [4] D-T reactivity,

- new definition of the "degrading" power used in the expression of the energy confinement time.

2.1. Fusion reactions

In the present version of the code, we only consider the D-T fusion reaction

$$D + T \longrightarrow {}^4He(3.56\ MeV) + n(14.03\ MeV) \quad [17.59\ MeV] \qquad (1)$$

For a 50-50 D-T plasma, the correction introduced by the contribution of the D-D and T-T reactivities can be estimated to be of the order of a few percents.

2.2. Geometry

2.2.1. Outer magnetic surface, plasma volume, poloidal section surface and plasma surface

In the case of a plasma poloidal cross-section with a strong triangularity and X-points, the elliptical approximation for the outer magnetic surface is no longer accurate for the calculation of the geometrical quantities. In the present version of the code, the outer magnetic surface is supposed to be sym-

etrical with respect to the equatorial plane and to have X-points. The elongation and triangularity at the separatrix are denoted κ_X and δ_X, a is the plasma horizontal minor radius, R is the major radius. The outer magnetic surface makes an angle ψ^+ with the horizontal plane at the external side of the torus and ψ^- at the internal side [Fig. 1]. The case of an outer magnetic surface with no X-points is recovered by making $\psi^+=\psi^-=0$. If the following conditions are satisfied, i.e.,

$$tg\psi^+ < \frac{\kappa_X}{2(1+\delta_X)} \qquad \text{and} \qquad tg\psi^- < \frac{\kappa_X}{2(1-\delta_X)} \tag{2}$$

the poloidal section of the outer magnetic surface may be modelled with portions of ellipses. The mathematical description of the outer surface in this case is given in Appendix A. In the frame of this model, it is possible to derive analytic expressions for the total plasma volume V, for the surface S_p of the poloidal cross-section and for the external plasma surface S. We obtain

$$V = 2\pi^2\kappa_X A a^3\, \Theta_V(\delta_X,\kappa_X,A,\psi^+,\psi^-) \tag{3}$$

where $A=R/a$ is the torus aspect ratio,

$$S_p = \pi\kappa_X a^2\, \Theta_{Sp}(\delta_X,\kappa_X,\psi^+,\psi^-) \tag{4}$$

and

$$S = 4\pi^2 A a^2 E_1(\kappa_X)\, \Theta_S(\delta_X,\kappa_X,A,\psi^+,\psi^-) \tag{5}$$

with

$$E_1(\kappa_X) = \frac{2}{\pi}\,\kappa_X\, E[(1-1/\kappa_X^2)^{1/2}] \tag{6}$$

where the function E is the complete elliptic integral of the second kind, and the explicit expressions for the factors Θ_V, Θ_{Sp}, and Θ_S are given in Appendix A. These quantities represent the corrections with respect to the case of an elliptic cross-section with no triangularity (and no X-points). For the ITER reference case ($A \simeq 2.79$, $\kappa_X=2.22$, $\delta_X=0.58$, $\psi^+=18°$, $\psi^-=68°$), we obtain $\Theta_V \simeq 0.89$, $\Theta_{Sp} \simeq 0.92$, $\Theta_S \simeq 0.94$, showing that the corrections are of the order of 10%.

2.2.2. Magnetic surfaces, radial integrations

For the volume and poloidal surface integrations, the magnetic surfaces are supposed to be similar to the outer magnetic surfaces [center O (no Shafranov shift), similarity factor ρ ($\rho=0$ at the magnetic axis, $\rho=1$ at the plasma boundary)]. For any function $F(\rho)$, we have

$$\frac{1}{V}\int_V F(\rho)\ dv = \frac{1}{1-\Theta_1/A}\int_0^1 F(\rho)\ (1-\frac{3}{2}\frac{\Theta_1}{A}\rho)\ 2\rho d\rho \qquad (7)$$

$$\frac{1}{S_p}\int_S F(\rho)\ ds = \int_0^1 F(\rho)\ 2\rho d\rho \qquad (8)$$

where $\Theta_1(\delta_X,\kappa_X,\psi^+,\psi^-)$ is given in Appendix A. The factor Θ_1 represents the correction to the volume integration introduced by the deformation of the magnetic surfaces relative to the pure elliptic case. The model for the shape of the surfaces is of course not physical, but it allows to introduce a simple mathematical consistency between the radial integrations and the volume calculation.

2.3. Safety factor

The cylindrical safety factor q_{cyl} at the magnetic surface where the poloidal flux is 95% of the total poloidal flux will be used. It is related to the total plasma current I_p flowing through the plasma by the relation [5]

$$q_{cyl} = \frac{2\pi}{\mu_o}\frac{1+K^2}{2}\frac{B_t a}{AI_p} \quad \text{with} \quad K^2 = \kappa^2(1+2\delta^2-1.2\delta^3) \qquad (9)$$

where B_t is the toroïdal magnetic field at the magnetic axis, and κ and δ are the elongation and triangularity at the 95% magnetic surface, respectively. The true safety factor q_ψ at the 95% magnetic surface is also used, it is related to q_{cyl} by the following fit:

$$q_\psi = q_{cyl}\frac{C_{q1}-C_{q2}/A}{(1-1/A^2)^2} \qquad (10)$$

where we take C_{q1}=1.17 and C_{q2}=0.65 [5].

2.4. Composition, impurities

The electron density is denoted n. In the present version of the code, we suppose a plasma with an equal mixture of D and T (n_D=n_T). Two light impurity species, with atomic numbers Z_1 and Z_2 are supposed to be present with an arbitrary ratio n_2/n_1=r_{21}. A fraction f_α=n_α/n of alpha particles is also assumed (Z_α=2). The resulting effective atomic number Z_{eff} is defined by the relation

$$Z_{eff} = \frac{\Sigma\ n_i Z_i^2}{\Sigma\ n_i Z_i} \qquad (11)$$

The impurity contents is completely determined if Z_1, Z_2, r_{21}, f_α, and Z_{eff} are given. We obtain

$$f_{DT} = \frac{n_D+n_T}{n} = \frac{Z_1(Z_1-Z_{eff})+r_{21}Z_2(Z_2-Z_{eff}) - 2[Z_1(Z_1-2)+r_{21}Z_2(Z_2-2)]f_\alpha}{Z_1(Z_1-1) + r_{21}Z_2(Z_2-1)} \quad (12)$$

$$f_1 = \frac{n_1}{n} = \frac{Z_{eff}-1-2f_\alpha}{Z_1(Z_1-1) + r_{21}Z_2(Z_2-1)} \quad (13)$$

$$f_2 = \frac{n_2}{n} = r_{21}\, f_1 \quad (14)$$

where f_{DT} is the fraction of D + T.

2.5. Temperatures

The electron temperature is denoted T. The deuterium, tritium as well as all the impurity species and the thermalized alpha particles are assumed to have the same temperature T_i. We note

$$\theta_i = \frac{T_i}{T} \quad (15)$$

2.6. Profiles, averaged values

The electron density and temperature profiles are supposed to have the following form:

$$n(\rho) = n_0(1-\rho^2)^{\alpha_n} \quad , \quad T(\rho) = T_0(1-\rho^2)^{\alpha_T} \quad (16)$$

where n_0 and T_0 are the values at the magnetic axis, and α_n and α_T are the profile peaking parameters. The volume averaged electron density <n> and the density averaged electron temperature [T] will be used. With the above profiles, we have

$$\langle n\rangle = \frac{1}{V}\int_V n\,dv = \frac{n_0}{1+\alpha_n}\,\frac{1-\Gamma_1(\alpha_n)\Theta_1/A}{1-\Theta_1/A} \quad (17)$$

$$[T] = \frac{\int_V nT\,dv}{\int_V n\,dv} = T_0\,\frac{1+\alpha_n}{1+\alpha_n+\alpha_T}\,\frac{1-\Gamma_1(\alpha_n+\alpha_T)\Theta_1/A}{1-\Gamma_1(\alpha_n)\Theta_1/A} \quad (18)$$

where the function Γ_1 is defined in Eq. (A.27).

The central horizontal line averaged electron density $\bar{n}$ defined by the relation

$$\bar{n} = \frac{\int_0^a n(x)\,dx}{a} \quad (19)$$

is generally used by experimentalists (in the expression of the density limit or of the energy confinement time). With the above profiles, we have the relation

$$\frac{\bar{n}}{\langle n\rangle}(\alpha_n,\frac{\Theta_1}{A}) = (1+\alpha_n)\,2^{2\alpha_n}\,\frac{\Gamma^2(1+\alpha_n)}{\Gamma(2+2\alpha_n)}\,\frac{1-\Theta_1/A}{1-\Gamma_1(\alpha_n)\Theta_1/A} \quad (20)$$

2.7. Thermal equilibrium

2.7.1. The thermal equilibrium equation

The following thermal equilibrium equation is solved numerically by the code:

$$P_\alpha(\langle n\rangle,[T]) + P_\Omega([T]) + P_{add} = P_B(\langle n\rangle,[T]) + P_t(\langle n\rangle,[T],P_{deg}) \qquad (21)$$

where P_α, P_Ω, P_{add} are the alpha, ohmic, and additional power sources and P_B, P_t the bremsstrahlung radiation and transport losses, respectively. The synchrotron radiation losses, which are neglected here, can be shown to be negligible for a realistic reflection coefficient of the wall and the operating temperatures which will be considered in the present paper (~ 10 keV). All the source and loss terms are integrated over the profiles given in Eq. (16).

By definition of the global energy confinement time τ_E, the transport loss P_t is expressed as

$$P_t(\langle n\rangle,[T],P_{deg}) = \frac{W_{th}(\langle n\rangle,[T])}{\tau_E(\langle n\rangle,P_{deg})} \qquad (22)$$

where W_{th} is the total energy content of the plasma and P_{deg} is the so-called "degrading" power. The expression of P_{deg} is as follows:

$$P_{deg} = P_{tot} - \varepsilon_r P_B \qquad (23)$$

with

$$P_{tot} = P_\alpha + P_\Omega + P_{add} \qquad (24)$$

The case ε_r=0 (P_{deg}=P_{tot}) was generally considered until recently. However if the degration of the confinement is supposed to be due to a [T] dependence of τ_E, it can be shown that ε_r=1 must be taken.

2.7.2. Alpha power source

The number N_f of D-T fusion reactions occuring in the plasma volume is

$$N_f = \int_V n_D n_T \overline{\sigma v}(T_i)\, dv \qquad (25)$$

where $\overline{\sigma v}(T_i)$ is the D-T thermonuclear reaction rate for two D and T maxwellian populations with the same temperature T_i. The expression used for $\overline{\sigma v}(T)$ is given in Appendix B. The alpha power source may be written as

$$P_\alpha = N_f F_\alpha E_\alpha \qquad (26)$$

where F_α is the fraction of the total generated alpha particle power which is delivered to the plasma (electrons and ions), and E_α is the initial kinetic energy of the alpha particle (3.56 MeV)[1]. Using the definition of Z_{eff}, the plasma quasi-neutrality, and the profiles in Eq. (16), it can be shown that

$$P_\alpha(<n>,[T]) = C_\alpha \frac{<n>^2}{4} \overline{\sigma v}^*([T])\ F_\alpha E_\alpha\ V \tag{27}$$

where $\overline{\sigma v}^*([T])$ is the profile averaged thermonuclear reaction rate, we obtain

$$\overline{\sigma v}^*([T],\theta_i,\alpha_n,\alpha_T,\frac{\Theta_1}{A}) = (1+\alpha_n)^2 \frac{1-\Theta_1/A}{[1-\Gamma_1(\alpha_n)\Theta_1/A]^2} \times \ldots$$

$$\times \int_0^1 (1-\rho^2)^{2\alpha_n} \overline{\sigma v}\left[\theta_i \frac{T_0}{[T]}[T](1-\rho^2)^{\alpha_T}\right] (1-\frac{3}{2}\frac{\Theta_1}{A}\rho)\ 2\rho d\rho \tag{28}$$

with $T_0/[T]$ given in Eq. (18). The integration in Eq. (28) is performed numerically. C_α is the dilution coefficient in the alpha power source due to the impurity and ^{4}He contents, we obtain

$$C_\alpha = \left[\frac{Z_1(Z_1-Z_{eff})+r_{z_1}Z_2(Z_2-Z_{eff}) - 2[Z_1(Z_1-2)+r_{z_1}Z_2(Z_2-2)]f_\alpha}{Z_1(Z_1-1)+r_{z_1}Z_2(Z_2-1)}\right]^2 \tag{29}$$

2.7.3. Ohmic power source

In the present version of the code, the local plasma resistivity is taken in the simplified following form:

$$\eta = \frac{\eta_0 Z_{eff}}{T^{3/2}} \tau_{NC}(A,\rho) \quad \text{with} \quad \eta_0 = 3\times10^{-8} \tag{30}$$

where

$$\tau_{NC}(A,\rho) = \frac{1}{1 - \frac{1.95}{A^{1/2}}\rho^{1/2} + \frac{0.95}{A}\rho} \tag{31}$$

is the local neo-classical resistivity enhancement factor. The ohmic power is given by

$$P_\Omega = \int_V \eta j^2\ dv \tag{32}$$

Assuming pure inductive current drive ($E=\eta j$), and a flat electric field E, the ohmic power may be written as

---

[1] Here the plasma kinetic energy is neglected in comparison with the initial alpha particle energy.

$$P_\Omega([T]) = \eta_o^* Z_{eff} \tau_{NC}^* \left[\frac{I_p}{S_p}\right]^2 \frac{1}{[T]^{3/2}} V \tag{33}$$

with S_p given in Eq. (4), and η_o^*, τ_{NC}^* given in Appendix C.

2.7.4. Additionnal power

The additional power source P_{add} is a constant in a 1/2-D model. Only ignition will be considered in the present paper (*i.e.* P_{add}=0).

2.7.5. Bremsstrahlung radiation loss

The non-relativistic Born approximation is used for the electron-ion bremsstrahlung loss, i.e.

$$P_B = \int_V C_B Z_{eff} n^2 T^{1/2} \, dv \tag{34}$$

with

$$C_B = \frac{1}{(4\pi\varepsilon_o)^3} \frac{32\sqrt{2}}{3\sqrt{\pi}} \frac{e^6 k^{1/2}}{m_e^{3/2} c^3 \hbar} \simeq 5.355\times10^{-37} \tag{35}$$

With the profiles in Eq. (16), we obtain

$$P_B(<n>,[T]) = C_B^* Z_{eff} <n>^2 [T]^{1/2} V \tag{36}$$

with

$$C_B^* = C_B \frac{(1+\alpha_n)^{3/2}(1+\alpha_n+\alpha_T)^{1/2}}{1+2\alpha_n+\alpha_T/2} \frac{[1-\Theta_i/A]\,[1-\Gamma_i(2\alpha_n+\alpha_T/2)\Theta_i/A]}{[1-\Gamma_i(\alpha_n)\Theta_i/A]^{3/2}[1-\Gamma_i(\alpha_n+\alpha_T)\Theta_i/A]^{1/2}} \tag{37}$$

The above expression has been checked by comparison with the numerical integration in Eq. (34).

2.7.6. Transport losses, energy confinement time scaling

For the multispecies and multi-temperature plasma considered here, the thermal energy content in Eq. (22) may be written as

$$W_{th}(<n>,[T]) = C_W \, 3<n>k[T] \, V \tag{38}$$

with

$$C_W = \tfrac{1}{2}(1+\theta_i) - \ldots$$
$$- \theta_i \frac{[Z_1-1+r_{21}(Z_2-1)](Z_{eff}-1)+[(Z_1-1)(Z_1-2)+r_{21}(Z_2-1)(Z_2-2)]f_\alpha}{2[Z_1(Z_1-1)+r_{21}Z_2(Z_2-i)]} \tag{39}$$

The expression of the global energy confinement time τ_E in terms of the plasma parameters is taken to be the mixed neo-Alcator/ITER-89P scaling following the Goldston prescription [6]:

$$\tau_E = \left[1/\tau_{ENA}^2 + 1/\tau_{EP}^2\right]^{-1/2} \tag{40}$$

where τ_{ENA} is the neo-Alcator scaling [7], we take

$$\tau_{ENA} = 7\times10^{-22}\ M_{eff}^{0.5}\ \bar{n}\ R^2 a\ q_{cyl} \tag{41}$$

and τ_{EP} is the ITER-89P monomial scaling [5]:

$$\tau_{EP} = f_L\ C_\tau\ \frac{M_{eff}^{0.5}\ \kappa_X^{0.5}\ I_p^{0.85}\ (\bar{n})^{0.1}\ B_t^{0.2}\ R^{1.2}\ a^{0.3}}{P_{deg}^{0.5}} \tag{42}$$

with

$$C_\tau = 4.8\times10^{-6.1} \simeq 3.81\times10^{-6} \tag{43}$$

In the above expression of τ_{EP}, M_{eff} is an effective atomic mass number of the plasma ions (for a 50-50 D-T plasma, M_{eff} is taken to be 2.5), and f_L is the so-called energy confinement time enhancement factor relative to the L-mode.

2.8. The operating window

2.8.1. Beta limit

We suppose that operation is restricted to the first MHD stability regime with the usual Troyon limit on beta, i.e. $\langle\beta\rangle < \langle\beta\rangle_T$ with

$$\langle\beta\rangle = C_W\ \frac{2\langle n\rangle k[T]}{B_t^2/2\mu_o} \tag{44}$$

where C_W is given in Eq. (39) and

$$\langle\beta\rangle_T = 10^{-8}\ g\ \frac{I_p}{B_t a} \tag{45}$$

where g is the Troyon parameter. The fast alpha contribution to beta is not considered in the present version of the code.

2.8.2. Density limit

The density at the edge is limited by a thermal instability of the outer plasma. A number of models have been recently proposed to quantify this limit [5]. In the present paper, the Greenwald limit [8] for the line averaged density is calculated but is not considered as a strong constraint. We have

$$\bar{n}_G = 10^{14}\ \kappa_X \frac{I_p}{S_p} \tag{46}$$

2.9. Other relations

A number of other constraints may be imposed to a machine. These constraints lead to additional relations between the physical parameters of the tokamak.

2.9.1. Maximum magnetic field inside the superconducting windings

Let B_{tmax} be the maximum toroidal magnetic field inside the superconducting windings, and d_{BS} be the thickness of the wall, inner part of the blanket, shield, cryostat, and coil mechanical structure, we have the relation

$$\frac{B_t}{B_{tmax}} = \frac{A-1-d_{BS}/a}{A} \tag{47}$$

2.9.2. Total fusion power

Let P_{fus} be the total fusion power (alpha particles plus neutrons) generated by the thermonuclear plasma, we have

$$P_{fus} = C_\alpha \frac{\langle n\rangle^2}{4} \overline{\sigma v}^*([T])\ (E_\alpha + E_n)\ V \tag{48}$$

2.9.3. Average neutron load at the plasma surface

Let Γ_n be the surface averaged neutron flux at the plasma surface, we have

$$\Gamma_n = C_\alpha \frac{\langle n\rangle^2}{4} \overline{\sigma v}^*([T])\ E_n \frac{V}{S} \tag{49}$$

where the surface S of the plasma is given in Eq. (5).

From Eqs. (48) and (49), we see that imposing both P_{fus} and Γ_n yields a simple necessary condition on the plasma radius, i.e.

$$a = \frac{1}{2\pi}\left[\frac{E_n}{E_\alpha + E_n}\right]^{1/2} \frac{1}{A^{1/2} E_i^{1/2} (\kappa_X) \Theta_S^{1/2}} \frac{P_{fus}^{1/2}}{\Gamma_n^{1/2}} \tag{50}$$

3. APPROXIMATE ANALYTICAL CRITERIA FOR IGNITION

Neglecting the ohmic power P_Ω at ignition, and supposing that $1/\tau_{ENA}^2$ is negligible in comparison with $1/\tau_{EP}^2$ in Eq. (40) (i.e. $\tau_E \simeq \tau_{EP}$), the thermal equilibrium equation [Eq. (21)] may be solved analytically [2]. Thence, different analytical conditions for ignition may be derived.

3.1. Criterion for ignition with imposed total fusion power

The condition for the ignition curve in the (<n>,[T]) plane to have at least one point of contact with the constant fusion power curve may be expressed explicitely. In the special case of the ITER-89P scaling and using a syntax similar to that of Ref. [10], this condition may be written as:

$$C_{igP}\, f_L\, F_\alpha^{0.5}\, F_{dilution}\, F_{peaking}\, F_{shape}\, P_{fus}^{0.05}\, \frac{M_{eff}^{0.5}}{q_\psi^{0.85}\, A^{0.2}}\, a^{0.7}\, B_t^{1.05} \geq 1 \qquad (51)$$

where

$$F_{dilution}(Z_{eff}, f_\alpha, Z_1, Z_2, r_{21}, \theta_i) = \frac{C_\alpha^{0.45}}{C_W} \qquad (52)$$

$$F_{peaking}(\alpha_n, \alpha_T, \theta_i, F_\alpha, Z_{eff}, C_\alpha, \frac{\Theta_i}{A}) = \frac{1}{\Sigma_P} \qquad (53)$$

$$F_{shape}(\kappa_X, \delta_X, \kappa, \delta, A, \psi^+, \psi^-) = \frac{1}{\kappa_X^{0.05}}\left[\frac{1+K^2}{2}\right]^{0.85} \frac{1}{\Theta_V^{0.55}} \left[\frac{C_{q1}-C_{q2}/A}{(1-1/A^2)^2}\right]^{0.85} \qquad (54)$$

with

$$C_{igP} = \frac{C_\tau\, E_\alpha^{0.5}}{3\times 2^{0.6}\pi^{0.25}\mu_o^{0.85} k\, (E_\alpha+E_n)^{0.05}} \simeq 1.16\times 10^9 \qquad (55)$$

and

$$\Sigma_P = \frac{1}{(\bar{n}/\langle n\rangle)^{0.1}}\, \min\left[[T]\, \frac{\{\overline{\sigma v}^*([T])-\varepsilon_r \delta_B^*[T]^{1/2}\}^{0.5}\, \overline{\sigma v}^{*0.05}([T])}{\overline{\sigma v}^*([T])-\delta_B^*[T]^{1/2}}\right] \qquad (56)$$

where

$$\delta_B^* = \frac{4 C_B^* Z_{eff}}{F_\alpha E_\alpha C_\alpha} \qquad (57)$$

C_α and C_W are given in Eqs. (29) and (39), Θ_V in Eq. (A.9); K, C_{q1} and C_{q2} are defined in Eqs. (9,10) and ε_r in Eq. (23). The minimum in Eq. (56) is calculated numerically as well as the $\overline{\sigma v}^*([T])$ function [Eq. (28)].

3.2. Criterion for ignition with imposed averaged neutron flux at the plasma surface

A similar condition may be written for the possibility of ignition at or below a given averaged neutron flux Γ_n at the plasma surface. This condition reads:

$$C_{ig\Gamma}\, f_L\, F_\alpha^{0.5}\, F_{dilution}\, F_{peaking}\, F'_{shape}\, \Gamma_n^{0.05}\, \frac{M_{eff}^{0.5}}{q_\psi^{0.85}\, A^{0.15}}\, a^{0.8}\, B_t^{1.05} \geq 1 \qquad (58)$$

where

$$F'_{shape}(\kappa_X,\delta_X,\kappa,\delta,A,\psi^+,\psi^-) = \frac{E_1^{0.05}(\kappa_X)}{\kappa_X^{0.05}}\left[\frac{1+K^2}{2}\right]^{0.85} \frac{\Theta_S^{0.05}}{\Theta_V^{0.55}} \left[\frac{C_{q1}-C_{q2}/A}{(1-1/A^2)^2}\right]^{0.85} \qquad (59)$$

with

$$C_{ig\Gamma} = \frac{C_\tau\, E_\alpha^{0.5}}{3\times 2^{0.5}\pi^{0.15}\mu_o^{0.85} k\, E_n^{0.05}} \simeq 1.41\times 10^9 \qquad (60)$$

and Θ_S is given in Eq. (A.14).

3.3. Criterion for ignition with constraints on B_{tmax}, d_{BS}, q_ψ, Γ_n, and P_{fus}

Imposing both the fusion power P_{fus} and the neutron flux Γ_n, together with the maximum magnetic field B_{tmax}, the distance d_{BS}, and the value of q_ψ, the condition for ignition may be written in the following form:

$$C_{igP\Gamma}\, f_L\, F_\alpha^{0.5}\, F_{dilution} F_{peaking} F''_{shape}\, \frac{P_{fus}^{0.4}}{\Gamma_n^{0.35}} \left[\frac{A-1-d_{BS}/a}{A}\right]^{1.05} \frac{M_{eff}^{0.5}}{q_\psi^{0.85}\, A^{0.55}}\, B_{tmax}^{1.05} = 1 \qquad (61)$$

where

$$F''_{shape}(\kappa_X,\delta_X,\kappa,\delta,A,\psi^+,\psi^-) = \frac{1}{\kappa_X^{0.05} E_1^{0.35}(\kappa_X)} \left[\frac{1+K^2}{2}\right]^{0.85} \frac{1}{\Theta_S^{0.35}\Theta_V^{0.55}} \left[\frac{C_{q1}-C_{q2}/A}{(1-1/A^2)^2}\right]^{0.85} \qquad (62)$$

with

$$C_{igP\Gamma} = \frac{C_\tau\, E_\alpha^{0.5}\, E_n^{0.35}}{3\times 2^{1.3}\pi^{0.95}\mu_o^{0.85} k\, (E_\alpha+E_n)^{0.4}} \simeq 2.97\times 10^8 \qquad (63)$$

In Eq. (61), a is supposed to be expressed in terms of A, P_{fus} and Γ_n by means of Eq. (50). With the above constraints and giving the shape of the poloidal section, we clearly see that the value of f_L calculated from Eq. (61) is only a function of the aspect ratio A.

3.4. Generalisation to an arbitrary monomial scaling

The generalisation of the three above conditions to a monomial scaling of the energy confinement time τ_E with arbitrary exponents, i.e.

$$\tau_E \simeq \tau_{EP} = f_L C_\tau \frac{M_{eff}^\mu\, \kappa_X^\chi\, I_p^\iota\, (\bar{n})^\nu\, B_t^\beta\, R^\rho\, a^\alpha}{P_{deg}^\omega} \qquad (64)$$

is given in Appendix D.

4. SENSITIVITY STUDY FOR THE ITER BASELINE MACHINE

4.1. The ITER reference parameters

The reference parameters for the ITER baseline machine [1] are as follows:

$$a = 2.15 \text{ m}, \; R = 6 \text{ m}, \; B_t = 4.85 \text{ T}, \; I_p = 22 \text{ MA} \tag{65}$$

$$\kappa_X = 2.22, \; \delta_X = 0.58, \; \kappa = 1.98, \; \delta = 0.39 \tag{66}$$

We take $\psi^+=18°$, $\psi^-=68°$ to represent the ITER plasma shape. The corresponding poloidal cross-section is represented in Fig. 1. We also assume:

$$\left| \begin{array}{l} T_i=T_e \; (\theta_i=1) \\ F_\alpha = 1, \; Z_{eff} = 1.7, \; f_\alpha = 10\%, \; Z_1 = 6 \; (C), \; r_{z1} = 0 \\ M_{eff} = 2.5, \; \alpha_n = 0.5, \; \alpha_T = 1 \end{array} \right. \tag{67}$$

The total fusion power for the baseline ITER project is taken to be

$$P_{fus} = 1100 \text{ MW} \tag{68}$$

The distance between the inner plasma boundary and the point with maximum toroidal magnetic field is taken from Ref. [9]:

$$d_{BS} = 1.127 \text{ m} \tag{69}$$

For the degrading power [Eq. (23)] in the ITER-89P scaling, we take $\varepsilon_r=1$.

With the above parameters, the following quantities may be calculated:

$$\left| \begin{array}{l} A \simeq 2.79, \; V \simeq 1080 \text{ m}^3, \; S_p \simeq 29.6 \text{ m}^2, \; S \simeq 803 \text{ m}^2 \\ \Gamma_n \simeq 1.09 \text{ MW/m}^2, \; q_{cyl} \simeq 2.48, \; q_\psi \simeq 3.06, \; B_{tmax} \simeq 10.7 \text{ T} \\ f_i \; (C) \simeq 1.67 \; \%, \; f_{DT} = 70 \; \%, \; C_\alpha = 0.49, \; C_W \simeq 0.908 \\ \frac{n_o}{\langle n \rangle} \simeq 1.49, \; \frac{T_o}{[T]} \simeq 1.66, \; \frac{\bar{n}}{\langle n \rangle} \simeq 1.17 \end{array} \right. \tag{70}$$

4.2. Ignition for the reference parameters

The ignition curves for the ITER reference parameters are represented in Fig. 2 for f_L= 1.84, 1.93, 2. The first two values correspond to contact of the ignition curve with the Troyon beta limit curve (g=3) and to the constant fusion power curve (P_{fus}=1100 MW or $\Gamma_n \simeq 1.09$ MW/m²), respectively. The Greenwald density limit is also indicated. The sensitivity of the ignition curve to the value of f_L is clearly illustrated. Disregarding the problem of thermal control of the burn, we also see that an optimum temperature exists for operation at

an imposed value of the total fusion power. In the present case, this temperature is $[T] \simeq 11$ keV and the corresponding enhancement factor is $f_L \simeq 1.93$.

4.3. Sensitivity of ignition to various plasma parameters and model hypothesis

4.3.1. Effect of the density profile peaking parameter

The minimum value of f_L (denoted f_{LP}) allowing ignition with a fixed fusion power P_{fus}=1100 MW has been represented in Fig. 3 as a function of the exponent α_n of the density profile. The full curve is the numerical result obtained with the HELIOS code, the dotted line represents the analytical criterion from Eq. (51). The optimum temperature $[T]_{opt}$ corresponding to the contact between the ignition curve and the curve P_{fus}=1100 MW is also plotted. The excellent agreement between numerical and analytical results is due to negligible ohmic power for the optimum plasma parameters and to the predominance of the degraded part in the expression (40) of the energy confinement time. We see that density profiles slightly flatter than assumed in the reference case lead to required values of f_L in excess of 2. The optimum temperature stays in the range 10-13 keV.

4.3.2. Effect of the temperature profile peaking parameter

The variation of f_{LP} as a function of the exponent α_T of the temperature profile has been plotted in Fig. 4 as well as the corresponding ignition temperature. Detrimental effect of temperature profiles slightly flatter than the reference parabolic case is also clearly seen. The optimum averaged temperature is strongly decreasing when peaking the temperature profile, as a consequence of enhanced nuclear reactivity in the central part of the plasma.

4.3.3. Effect of dilution due to alpha particles

The variation of f_{LP} as a function of the fraction f_α of the helium ashes in the plasma is represented in Fig. 5 (with Z_{eff}=1.7 kept constant). For f_α=12%, the critical f_L=2 value is overshot.

4.3.4. Effect of carbon contamination

The variation of f_{LP} as a function of Z_{eff} (with f_α=10% kept constant) is represented in Fig. 6. We see that f_L=2 is exceeded for $Z_{eff} > 1.8$.

4.3.5. Effect of the ratio Te/Ti

The variation of f_{LP} as a function of the ratio T_e/T_i is represented in Fig. 7. An ion temperature 6% lower than the electron one would make the required value of f_L greater than 2.

4.3.6. Effect of the hypothesis on the degrading power

The variation of f_{LP} as a function of the parameter ε_r in Eq. (23) is represented in Fig. 8. If the bremsstrahlung radiated power is not substracted from the total power in the calculation of the degrading power (ε_r=0 instead of ε_r=1), the required value of f_L is also found to be in excess of 2.

From the results of the above sensitivity analysis, it can be concluded that the safety margin of the ITER baseline project is not sufficient.

5. OPTIMIZATION OF ITER

5.1. Optimization of the aspect ratio for fixed values of P_{fus}, Γ_n, B_{tmax}, d_{BS}, and q_ψ

We suppose that the total fusion power and the averaged neutron flux at the plasma surface are imposed. We take the ITER reference values:

$$P_{fus} = 1100 \text{ MW} \quad , \quad \Gamma_n \simeq 1.09 \text{ MW/m}^2 \tag{71}$$

In the present analysis, the heat load on the divertor plates is not explicitely constrained, however, imposing a constant value of the averaged neutron flux is equivalent to imposing a constant value of the mean thermal flux on the divertor plates since the total heat loss is proportional to the neutron loss, and the surface of the divertor plates is proportional to the plasma surface (for a given poloidal shape).

The maximum magnetic field in the superconducting windings is also supposed to be given. In the axisymmetrical approximation, this field is obtained in the equatorial plane on the outer surface of the windings at a distance d_{BS} from the plasma surface. For ITER we take [Eqs. (69), (70)]

$$d_{BS} = 1.127 \text{ m} \quad , \quad B_{tmax} \simeq 10.7 \text{ T} \tag{72}$$

The width d_{BS} is supposed to be the same for all aspect ratios. The shape of the poloidal section of the plasma (κ_X, δ_X, κ, δ, ψ^+, ψ^-), is also supposed to be unchanged, the values given in Eq. (66) being retained. The 95% safety factor q_ψ is supposed to be fixed, we take the ITER value [Eq. (70)]

$$q_\psi \simeq 3.06 \tag{73}$$

With the above constraints, the value of f_{LP} is only a function of the aspect ratio A as is now explained. Given A, the value of a is given by Eq. (50). The major radius follows (R = Aa). The toroidal magnetic field is then given by Eq. (47). The total plasma current may now be deduced from Eq. (9). At this point, all the macroscopic parameters of the plasma are known so that f_{LP} may be computed

as described in section 4.2. Results for the above numerical parameters and A varying from 2.79 to 5 are given in Table I.

TABLE I. Optimization of ITER aspect ratio for given P_{fus} (1100 MW) and Γ_n (1.09 MW/m²).

A	2.79	3	3.46	4	4.5	5
a (m)	2.15	2.07	1.92	1.78	1.68	1.59
R (m)	6.00	6.21	6.65	7.13	7.55	7.95
B_t (T)	4.85	5.19	5.79	6.33	6.71	7.03
I_p (MA)	22.0	20.6	17.9	15.4	13.6	12.0
f_{LP}	1.93	1.91	1.90	1.91	1.93	1.97
V (m³)	1080	1040	964	893	839	795
$\langle n \rangle (10^{20} m^{-3})$	1.13	1.15	1.19	1.23	1.27	1.30
[T] (keV)	11.4	11.4	11.5	11.5	11.5	11.5
g	1.89	1.86	1.84	1.89	1.96	2.06
$\bar{n}/\bar{n}_G$	0.801	0.807	0.828	0.859	0.892	0.926

We see that the enhancement factor is minimum for a finite value of the aspect ratio (A ≃ 3.46). Increasing A allows larger magnetic fields, but the constraints on P_{fus} and Γ_n result in smaller values of the minor radius and plasma current which in turn degrade the confinement. As the minimum of the function $f_{LP}(A)$ is very flat (Fig. 9), choosing A=2.79 does make a big difference as far as confinement is concerned. In the same way, choosing large value of A (if the ITER-89P scaling law for τ_E is confirmed to be extrapolable to such values [5]) is not a serious drawback. This result could be considered in support to large aspect ratios, which can be shown to be more favourable when constraints relative to steady state operation are included in the analysis [1].

5.2. Variation of the total fusion power

Repeating the above aspect ratio optimization for increasing values of P_{fus} (see Fig. 9) yields the results given in Table II below

TABLE II. Parameters of an ITER-like machine at the optimum aspect ratio for increasing values of P_{fus}.

P_{fus}(MW)	1100	1700	2200	3500
A	3.46	3.01	2.77	2.40
f_{LP}	1.90	1.49	1.29	1.01
a (m)	1.92	2.57	3.05	4.15
R (m)	6.65	7.73	8.46	9.96
B_t(T)	5.79	5.57	5.41	5.02
I_p(MA)	17.9	27.4	35.1	54.7
V (m^3)	964	2000	3070	6670
$\langle n \rangle (10^{20} m^{-3})$	1.19	1.02	0.939	0.803
[T] (keV)	11.5	11.5	11.5	11.5
q	1.84	1.45	1.27	1.02
$\bar{n}/\bar{n}_G$	0.828	0.835	0.843	0.858

We see that the optimum value of A is decreasing with increasing fusion power but the minimum is always very flat. For a 1700 MW machine, the minimum value of f_L is about 1.5; for a 2200 MW device, it is about 1.3. L-mode ignition is possible only with a 3500 MW machine. Note that the optimum temperature is constant and that Troyon and Greenwald conditions are always satisfied.

For comparison, the same curves have been represented in Fig. 10 in the case of Goldston scaling [6]. Increasing the aspect ratio is always favourable with this latter scaling.

5.3. Ignition curves in a 1700 MW ITER-like machine

Now, we consider in more details the machines corresponding to P_{fus}=1700 MW. The tokamak described in Table II is optimised to ignite at the lowest possible value of f_L with the constraints given in Eqs. (71, 72, 73) for Γ_n, d_{BS}, B_{tmax}, q_ψ and the poloidal cross-section shape described in Eq. (66).

Taking advantage of the interest of large aspect ratios for current drive issues, it is also worth considering the possibility of a machine with A=4 keeping

the same fusion power and the same constraints. The parameters of such a tokamak are found to be

$$a \simeq 2.22 \text{ m} \ , \ R \simeq 8.87 \text{ m} \ , \ I_p \simeq 20.2 \text{ MA} \ , \ B_t \simeq 6.66 \text{ T} \ , \ V \simeq 1720 \text{ m}^3$$

Ignition in this machine is obtained for $f_L \simeq 1.52$ which is very close to the optimal value f_L=1.49 obtained for $A \simeq 3$. It is also interesting to note that the enhanced maximum magnetic field allowed by larger aspect ratios ($B_{tmax} \simeq 13.3$ T in Ref. [1]) is also a favourable effect which has not been taken into account here.

The ignition curves corresponding to the latter machine are plotted in Fig. 11 for f_L=1.55, 1.52, and 1.48 corresponding to operations at $P_{fus} \simeq 1100$ MW ($\Gamma_n \simeq 0.707$ MW/m²), P_{fus}=1700 MW ($\Gamma_n \simeq 1.09$ MW/m²), and P_{fus}=3000 MW ($\Gamma_n \simeq 1.93$ MW/m²), respectively.

6. CONCLUSION

Operation of the ITER baseline machine (aspect ratio A=2.79), with a total fusion power of 1100 MW is found to require a minimum value $f_L \simeq 1.93$ of the enhancement factor with respect to the ITER-89P scaling of the confinement time.

Minor deviations with respect to the reference assumptions for the ash or impurity contents, density and temperature profiles, ratio of electron to ion temperatures, as well as alternate definitions of the degrading power, result in values of the required enhancement factor in excess of 2.

Considering the above insufficient safety margin, optimization of the aspect ratio has been performed for given values of the maximum magnetic field, blanket plus shield width, safety factor at the edge, averaged neutron flux at the plasma surface, and total fusion power. For the ITER reference values of these constraints, the optimum aspect ratio is found to be A=3.5, but it corresponds to only a marginal improvement of f_L (1.90).

A reasonable safety margin ($f_L \simeq 1.5$) is obtained by increasing the total fusion power up to 1700 MW, the corresponding optimum aspect ratio being shifted to A=3. On the basis of the relative insensitivity of the confinement constraints with respect to the value of the aspect ratio and of the advantage of large values of A for continuous operation issues, a machine with P_{fus}=1700 MW and A=4 has been described. Operation in this machine with f_L in the range 1.4-1.6 allows the production of a neutron wall load in the range 0.7-2 MW/m².

ACKNOWLEGMENTS

The author is grateful to Dr. LAURENT for fruitful discussions and careful reading of the manuscript.

APPENDIX A

Model for the geometry

If conditions (2) are satisfied, the outer magnetic surface may be represented with portions of ellipses. Introducing $\xi=x/a$ and $\zeta=z/a$, we obtain the following parametric equations for the outer poloidal section:

$$\begin{cases} \xi = \alpha_o^+ + \alpha^+\cos\theta \\ \zeta = \beta^+\sin\theta \end{cases} \qquad \text{for} \qquad -\theta_X^+ < \theta < \theta_X^+ \tag{A.1}$$

$$\begin{cases} \xi = \alpha_o^- + \alpha^-\cos\theta \\ \zeta = \beta^-\sin\theta \end{cases} \qquad \text{for} \qquad \theta_X^- < \theta < 2\pi-\theta_X^- \tag{A.2}$$

with

$$\theta_X^+ = \frac{\pi}{2} - \arcsin\frac{t^+}{1-t^+} = \arcsin\frac{(1-2t^+)^{1/2}}{1-t^+} \tag{A.3}$$

$$\theta_X^- = \frac{\pi}{2} + \arcsin\frac{t^-}{1-t^-} = \pi - \arcsin\frac{(1-2t^-)^{1/2}}{1-t^-} \tag{A.4}$$

$$\alpha_o^+ = -\frac{\delta_X+(1-\delta_X)t^+}{1-2t^+} \quad , \quad \alpha_o^- = \frac{-\delta_X+(1+\delta_X)t^-}{1-2t^-} \tag{A.5}$$

$$\alpha^+ = (1+\delta_X)\frac{1-t^+}{1-2t^+} \quad , \quad \alpha^- = (1-\delta_X)\frac{1-t^-}{1-2t^-} \tag{A.6}$$

$$\beta^+ = \kappa_X\frac{1-t^+}{(1-2t^+)^{1/2}} \quad , \quad \beta^- = \kappa_X\frac{1-t^-}{(1-2t^-)^{1/2}} \tag{A.7}$$

where

$$t^+ = \frac{1+\delta_X}{\kappa_X}\,\mathrm{tg}\psi^+ \quad , \quad t^- = \frac{1-\delta_X}{\kappa_X}\,\mathrm{tg}\psi^- \tag{A.8}$$

The explicit expressions of the factors Θ_V, Θ_{Sp}, Θ_S, Θ_1 in Eqs. (3, 4, 5, 7) are as follows:

- Volume

$$\Theta_V = \frac{1+\delta_X}{2}\frac{(1-t^+)^2}{(1-2t^+)^{3/2}}\left[1-\frac{1}{A}\frac{\delta_X+(1-\delta_X)t^+}{1-2t^+}\right]\mathrm{arc}(t^+) + \ldots$$

$$+\frac{1-\delta_X}{2}\frac{(1-t^-)^2}{(1-2t^-)^{3/2}}\left[1+\frac{1}{A}\frac{-\delta_X+(1+\delta_X)t^-}{1-2t^-}\right]\mathrm{arc}(t^-) + \frac{2}{3\pi}\frac{1}{A}\left[\frac{(1+\delta_X)^2}{1-2t^+} - \frac{(1-\delta_X)^2}{1-2t^-}\right] \tag{A.9}$$

where

$$\mathrm{arc}(t) = 1 - \frac{2}{\pi}\arcsin\frac{t}{1-t} - \frac{2}{\pi}\frac{t(1-2t)^{1/2}}{(1-t)^2} \tag{A.10}$$

In the special case $\psi^+=\psi^-=0$ (no X-points), we obtain

$$\Theta_V = 1 - (1-\frac{8}{3\pi})\frac{\delta_X}{A} \tag{A.11}$$

- Poloidal surface

$$\Theta_{Sp} = \frac{1+\delta_X}{2}\frac{(1-t^+)^2}{(1-2t^+)^{3/2}}\,\mathrm{arc}(t^+) + \frac{1-\delta_X}{2}\frac{(1-t^-)^2}{(1-2t^-)^{3/2}}\,\mathrm{arc}(t^-) \tag{A.12}$$

In the special case $\psi^+=\psi^-=0$, we obtain $\Theta_{Sp}=1$ independent of the triangularity.

- Plasma surface

Introducing

$$\kappa^+ = \frac{\kappa_X}{1+\delta_X} \quad , \quad \kappa^- = \frac{\kappa_X}{1-\delta_X} \tag{A.13}$$

we have

$$\Theta_S = \Theta_S^+ + \Theta_S^- \tag{A.14}$$

where

$$\Theta_S^+ = \frac{\kappa_X}{\pi E_1(\kappa_X)}\frac{1-t^+}{(1-2t^+)^{1/2}}\left[(1-\frac{1}{A}\frac{\delta_X+(1-\delta_X)t^+}{1-2t^+})E\left[\theta_X^+,(1-\frac{1}{(1-2t^+)\kappa^{+2}})^{1/2}\right] + \ldots\right.$$

$$\left. + \frac{1}{A}\frac{1+\delta_X}{2}\frac{1}{(1-2t^+)^{1/2}}\left[\frac{(t^{+2}+1/\kappa^{+2})^{1/2}}{1-t^+} + \frac{1-t^+}{(1-2t^+-1/\kappa^{+2})^{1/2}}\arcsin\frac{(1-2t^+-1/\kappa^{+2})^{1/2}}{1-t^+}\right]\right] \tag{A.15}$$

for

$$0 \le \mathrm{tg}\psi^+ \le \frac{\kappa^+}{2} - \frac{1}{2\kappa^+} \tag{A.16}$$

$$\Theta_S^+ = \frac{1+\delta_X}{\pi E_1(\kappa_X)} \frac{1-t^+}{1-2t^+}\left[(1-\frac{1}{A}\frac{\delta_X+(1-\delta_X)t^+}{1-2t^+})\left[E\{[1-(1-2t^+)\kappa^{+2}]^{\frac{1}{2}}\}-E\{\frac{\pi}{2}-\theta_X^+,[1-(1-2t^+)\kappa^{+2}]^{\frac{1}{2}}\}\right] + \ldots\right.$$

$$\left. + \frac{\kappa_X}{2A}\left[\frac{(t^{+2}+1/\kappa^{+2})^{\frac{1}{2}}}{1-t^+} + \frac{1-t^+}{(2t^+-1+1/\kappa^{+2})^{\frac{1}{2}}} \ln\frac{(t^{+2}+1/\kappa^{+2})^{\frac{1}{2}} + (2t^+-1+1/\kappa^{+2})^{\frac{1}{2}}}{1-t^+}\right]\right] \quad (A.17)$$

for

$$\frac{\kappa^+}{2} - \frac{1}{2\kappa^+} \leq tg\psi^+ < \frac{\kappa^+}{2} \quad (A.18)$$

and

$$\Theta_S^- = \frac{\kappa_X}{\pi E_1(\kappa_X)} \frac{1-t^-}{(1-2t^-)^{\frac{1}{2}}}\left[(1+\frac{1}{A}\frac{-\delta_X+(1+\delta_X)t^-}{1-2t^-})E\left[\pi-\theta_X^-,(1-\frac{1}{(1-2t^-)\kappa^{-2}})^{\frac{1}{2}}\right] - \ldots\right.$$

$$\left. - \frac{1}{A}\frac{1-\delta_X}{2}\frac{1}{(1-2t^-)^{\frac{1}{2}}}\left[\frac{(t^{-2}+1/\kappa^{-2})^{\frac{1}{2}}}{1-t^-} + \frac{1-t^-}{(1-2t^--1/\kappa^{-2})^{\frac{1}{2}}} \arcsin\frac{(1-2t^--1/\kappa^{-2})^{\frac{1}{2}}}{1-t^-}\right]\right] \quad (A.19)$$

for

$$0 \leq tg\psi^- \leq \frac{\kappa^-}{2} - \frac{1}{2\kappa^-} \quad (A.20)$$

$$\Theta_S^- = \frac{1-\delta_X}{\pi E_1(\kappa_X)} \frac{1-t^-}{1-2t^-}\left[(1+\frac{1}{A}\frac{-\delta_X+(1+\delta_X)t^-}{1-2t^-})\left[E\{[1-(1-2t^-)\kappa^{-2}]^{\frac{1}{2}}\}-E\{\theta_X^- - \frac{\pi}{2},[1-(1-2t^-)\kappa^{-2}]^{\frac{1}{2}}\}\right] - \ldots\right.$$

$$\left. - \frac{\kappa_X}{2A}\left[\frac{(t^{-2}+1/\kappa^{-2})^{\frac{1}{2}}}{1-t^-} + \frac{1-t^-}{(2t^--1+1/\kappa^{-2})^{\frac{1}{2}}} \ln\frac{(t^{-2}+1/\kappa^{-2})^{\frac{1}{2}} + (2t^--1+1/\kappa^{-2})^{\frac{1}{2}}}{1-t^-}\right]\right] \quad (A.21)$$

for

$$\frac{\kappa^-}{2} - \frac{1}{2\kappa^-} \leq tg\psi^- < \frac{\kappa^-}{2} \quad (A.22)$$

In the above expressions, $E(\varphi,k)$ is the incomplete elliptic integral of the second kind [11].

- Volume integration

$$\Theta_1 = \frac{1}{\Theta_{Sp}}\left[\frac{1+\delta_X}{2}\,\frac{(1-t^+)^2[\delta_X+(1-\delta_X)t^+]}{(1-2t^+)^{5/2}}\,\mathrm{arc}(t^+) - \frac{1-\delta_X}{2}\,\frac{(1-t^-)^2[-\delta_X+(1+\delta_X)t^-]}{(1-2t^-)^{5/2}}\,\mathrm{arc}(t^-) - \ldots\right.$$

$$\left. - \frac{2}{3\pi}\left[\frac{(1+\delta_X)^2}{1-2t^+} - \frac{(1-\delta_X)^2}{1-2t^-}\right]\right] \qquad (A.23)$$

In the special case $\psi^+=\psi^-=0$, we obtain

$$\Theta_1 = (1-\frac{8}{3\pi})\delta_X \qquad (A.24)$$

The following general relation between Θ_V, Θ_{Sp}, and Θ_1 holds

$$\Theta_V = \Theta_{Sp}(1-\frac{\Theta_1}{A}) \qquad (A.25)$$

The following relation will also be used

$$\frac{1}{V}\int_V (1-\rho^2)^\alpha \, dv = \frac{1}{1+\alpha}\,\frac{1-\Gamma_1(\alpha)\Theta_1/A}{1-\Theta_1/A} \qquad (A.26)$$

with

$$\Gamma_1(\alpha) = \frac{3\sqrt{\pi}}{4}\,\frac{\Gamma(\alpha+2)}{\Gamma(\alpha+5/2)} = 3\times 2^{2\alpha+1}\,\frac{\Gamma^2(\alpha+2)}{\Gamma(2\alpha+4)} \qquad [\Gamma_1(0) = 1] \qquad (A.27)$$

where Γ is the Euler gamma function.

N.B.: All the above analytic expressions have been checked by comparison with the numerical calculation of the integral expressions of the related quantities.

APPENDIX B

Fit for the D-T thermonuclear reaction rate

The D-T reaction rate $\overline{\sigma v}(T)$ used in the code is the fit, based on recent measurements, recently proposed by Sadler and van Belle [4]. The fit may be written as

$$\overline{\sigma v}(T) = \frac{a}{T^{2/3}}\,\frac{1}{U^{5/6}}\,\exp(-\frac{b}{T^{1/3}}\,U^{1/3}) \qquad (B.1)$$

where

$$a = \frac{P_1 B^{1/3}}{2^{1/3}(\mu c^2)^{1/2}_{keV}} \simeq 2.566327\times 10^{-18} \qquad (B.2)$$

$$b = \frac{3B^{2/3}}{2^{2/3}} \simeq 19.98303 \qquad (B.3)$$

$$U(T) = 1 - T\,\frac{P_2 + (P_4+P_6T)T}{1 + (P_3+P_5T)T} \tag{B.4}$$

where μ is the deuterium-tritium reduced mass [$\mu=m_Dm_T/(m_D+m_T)$], and

$$(\mu c^2)_{keV} = 1.124656\times10^6 \text{ keV} \;,\; B = 34.3827025 \text{ keV}^{\frac{1}{2}} \tag{B.5}$$

$$\left|\begin{array}{l} P_1 = 1.0545128\times10^{-15} \;,\; P_2 = 2.5077133\times10^{-2} \;,\; P_3 = 6.6024089\times10^{-2} \;, \\ P_4 = 2.5773408\times10^{-3} \;,\; P_5 = 8.1215505\times10^{-3} \;,\; P_6 = -6.1880463\times10^{-5} \end{array}\right. \tag{B.6}$$

APPENDIX C

Ohmic power

The ohmic power with the assumptions given in section 2.7.3 is given by Eq. (33) with

$$\eta_o^* = \eta_o\,\frac{(1+\alpha_n)^{3/2}(1+3\alpha_T/2)}{(1+\alpha_n+\alpha_T)^{3/2}}\,\frac{[1-\Gamma_1(3\alpha_T/2)\Theta_1/A]\,[1-\Gamma_1(\alpha_n+\alpha_T)\Theta_1/A]^{3/2}}{[1-\Theta_1/A]\,[1-\Gamma_1(\alpha_n)\Theta_1/A]^{3/2}} \tag{C.1}$$

and

$$\begin{aligned} \gamma^*_{NC}(A,\alpha_T,\Theta_1) = \Bigg[& 1 - \frac{1.95}{A^{1/2}}\,(1+\tfrac{3}{2}\alpha_T)\,\frac{B(1+3\alpha_T/2,\tfrac{5}{4}) - \tfrac{3}{2}\,B(1+3\alpha_T/2,\tfrac{7}{4})\Theta_1/A}{1-\Gamma_1(3\alpha_T/2)\Theta_1/A} + \cdots \\ & + \frac{0.95}{A}\,(1+\tfrac{3}{2}\alpha_T)\,\frac{B(1+3\alpha_T/2,\tfrac{3}{2}) - \tfrac{3}{2}\,B(1+3\alpha_T/2,2)\Theta_1/A}{1-\Gamma_1(3\alpha_T/2)\Theta_1/A}\Bigg] \times \cdots \\ & \times \left[1 - \frac{1.95}{A^{1/2}}\,\Gamma(\tfrac{5}{4})\,\frac{\Gamma(2+3\alpha_T/2)}{\Gamma(\frac{9}{4}+3\alpha_T/2)} + \frac{0.95}{A}\,\Gamma(\tfrac{3}{2})\,\frac{\Gamma(2+3\alpha_T/2)}{\Gamma(\frac{5}{2}+3\alpha_T/2)}\right]^{-2} \end{aligned} \tag{C.2}$$

where

$$B(x,y) = \frac{\Gamma(x)\Gamma(y)}{\Gamma(x+y)} \tag{C.3}$$

is the beta function [11]. γ^*_{NC} is the profile averaged neo-classical resistivity enhancement factor. A typical value is $\gamma^*_{NC}(A=3,\alpha_T=1,\Theta_1=0.0862) \simeq 2.58$. The above expression has been checked by comparison with the numerical integration in Eq. (32).

APPENDIX D

Ignition conditions for a general monomial scaling

With the same approximations as explained in section 3 and taking a general monomial scaling of the energy confinement time [Eq. (64)], the analytical conditions for ignition, Eqs. (51), (58), (61) become:

1/ Ignition for a given value of the total fusion power

$$C_{igP}\, f_L\, F_\alpha^{1-\omega}\, F_{dilution}\, F_{peaking}\, F_{shape}\, P_{fus}^{\frac{1-2\omega+\nu}{2}} \times \ldots \times \frac{M_{eff}^{\mu}}{q_\psi^{\iota}\, A^{\frac{1+\nu+2\iota-2\rho}{2}}}\, a^{\frac{2\iota+2\rho+2\alpha-3\nu-3}{2}}\, B_t^{\iota+\beta} \geq 1 \qquad (D.1)$$

where

$$F_{dilution}(Z_{eff}, f_\alpha, Z_1, Z_2, r_{21}, \theta_i) = \frac{C_\alpha^{\frac{1-\nu}{2}}}{C_W} \qquad (D.2)$$

$$F_{peaking}(\alpha_n, \alpha_T, \theta_i, F_\alpha, Z_{eff}, C_\alpha, \frac{\Theta_i}{A}) = \frac{1}{\Sigma_P} \qquad (D.3)$$

$$F_{shape}(\kappa_X, \delta_X, \kappa, \delta, A, \psi^+, \psi^-) = \frac{1}{\kappa_X^{\frac{1+\nu-2\chi}{2}}} \left[\frac{1+K^2}{2}\right]^{\iota} \frac{1}{\Theta_V^{\frac{1+\nu}{2}}} \left[\frac{C_{q1}-C_{q2}/A}{(1-1/A^2)^2}\right]^{\iota} \qquad (D.4)$$

with

$$C_{igP} = \frac{C_\tau\, E_\alpha^{1-\omega}}{3\times 2^{\frac{3-\nu-2\iota}{2}}\, \pi^{1+\nu-\iota}\, \mu_o^{\iota}\, k\, (E_\alpha+E_n)^{\frac{1-2\omega+\nu}{2}}} \qquad (D.5)$$

and

$$\Sigma_P = \frac{1}{(\bar{n}/\langle n\rangle)^{\nu}} \min\left[[T]\, \frac{\{\overline{\sigma v}^*([T])-\varepsilon_r \delta_B^*[T]^{\frac{1}{2}}\}^{\omega}\, \overline{\sigma v}^{*\,\frac{1-2\omega+\nu}{2}}([T])}{\overline{\sigma v}^*([T])-\delta_B^*[T]^{\frac{1}{2}}}\right] \qquad (D.6)$$

2/ Ignition for a given value of the averaged neutron flux at the plasma surface

$$C_{ig\Gamma}\, f_L\, F_\alpha^{1-\omega}\, F_{dilution}\, F_{peaking}\, F'_{shape}\, \Gamma_n^{\frac{1-2\omega+\nu}{2}} \times \ldots \times \frac{M_{eff}^{\mu}}{q_\psi^{\iota}\, A^{\omega+\iota-\rho}}\, a^{\frac{2\iota+2\rho+2\alpha-4\omega-\nu-1}{2}}\, B_t^{\iota+\beta} \geq 1 \qquad (D.7)$$

where

$$F'_{shape}(\kappa_X, \Gamma_X, \kappa, \Gamma, A, \psi^+, \psi^-) = \frac{E_1^{\frac{1-2\omega+\nu}{2}}}{\kappa_X^{\frac{1+\nu-2\chi}{2}}} \left[\frac{1+K^2}{2}\right]^{\iota} \frac{\Theta_S^{\frac{1-2\omega+\nu}{2}}}{\Theta_V^{\frac{1+\nu}{2}}} \left[\frac{C_{q1}-C_{q2}/A}{(1-1/A^2)^2}\right]^{\iota} \qquad (D.8)$$

and

$$C_{igI\Gamma} = \frac{C_\tau \, E_\alpha^{1-\omega}}{3\times 2^{\frac{1+4\omega-3\nu-2\iota}{2}} \, \pi^{2\omega-\iota} \, \mu_o^\iota \, k \, E_n^{\frac{1-2\omega+\nu}{2}}} \qquad (D.9)$$

3/ Ignition for given values of the fusion power, neutron flux at the plasma surface, maximum magnetic field, blanket plus shield width, and edge safety factor

$$C_{igPI\Gamma} \, f_L \, F_\alpha^{1-\omega} \, F_{dilution} \, F_{peaking} \, F''_{shape} \, \frac{P_{fus}^{\frac{2\iota+2\rho+2\alpha-4\omega-\nu-1}{4}}}{\Gamma_n^{\frac{2\iota+2\rho+2\alpha-3\nu-3}{4}}} \times \cdots$$

$$\times \left[\frac{A-1-d_{BS}/a}{A}\right]^{\iota+\beta} \frac{M_{eff}^{\mu}}{q_\psi^\iota \, A^{\frac{6\iota-2\rho+2\alpha-\nu-1}{4}}} \, B_{tmax}^{\iota+\beta} = 1 \qquad (D.10)$$

where

$$F''_{shape}(\kappa_X,\delta_X,\kappa,\delta,A,\psi^+,\psi^-) = \frac{1}{\kappa_X^{\frac{1+\nu-2\chi}{2}}} \left[\frac{1+K^2}{2}\right]^\iota \frac{1}{(E_i\Theta_S)^{\frac{2\iota+2\rho+2\alpha-3\nu-3}{4}} \, \Theta_V^{\frac{1+\nu}{2}}} \times \cdots$$

$$\times \left[\frac{C_{q1}-C_{q2}/A}{(1-1/A^2)^2}\right]^\iota \qquad (D.11)$$

$$C_{igPI\Gamma} = \frac{C_\tau \, E_\alpha^{1-\omega} \, E_n^{\frac{2\iota+2\rho+2\alpha-3\nu-3}{4}}}{3\times 2^{\rho+\alpha-2\nu} \, \pi^{\frac{2\rho+2\alpha-\nu-1}{2}} \, \mu_o^\iota \, k \, (E_\alpha+E_n)^{\frac{2\iota+2\rho+2\alpha-4\omega-\nu-1}{4}}} \qquad (D.12)$$

and where a is supposed to be given by Eq. (50).

REFERENCES

[1] ITER Parametric Analysis and Operational Performance, ITER Documentation Series No. 22, IAEA, Vienna (1991).

[2] JOHNER, J., "Thermonuclear Ignition in the Next-Generation Tokamaks," Fusion Technology, **19**, 515 (1991).

[3] JOHNER, J., "Ignition in the Next-Step Tokamak," Revue Générale Nucléaire, **1**, 51 (1991).

[4] SADLER, G., VAN BELLE, P., "An improved formulation of the D(t,n)^{4}He reaction cross-section", JET-IR(87)08, 1987.

[5] ITER Physics, ITER Documentation Series No. 21, IAEA, Vienna (1991).

[6] GOLDSTON, R.J., Plasma Phys. Controlled Fusion **26** (1984) 87.

[7] INTOR Group, International Tokamak Reactor, Phase Two A, Part II (Rep. Int. Workshop Vienna, 1984 and 1985), IAEA, Vienna (1986) 494.

[8] GREENWALD, M., TERRY, J., WOLFE, S., EJIMA, S., BELL, M., KAYE, S., NEILSON, G.H., "A New Look at Density Limits in Tokamaks", Plasma Fusion Center (MIT) Report PFC/JA-86-22, January 1988.

[9] ANE, J.-M., HERTOUT, P., ALLIBERT, J.-P., "Ignition in ITER", P/EM 91-09, February 1991.

[10] LAURENT, L., CHATELIER, M., GHENDRIH, P., JOHNER, J., ROUBIN, J.-P., "Problems Related to Ignition in the Next Step Tokamak", EUR-CEA-FC-1418, March 1991.

[11] GRADSHTEYN, I.S, RYZHIK, I.M., "Table of Integrals, Series, and Products", Academic Press, 1980.

FIGURES CAPTIONS

Fig. 1. ITER plasma poloidal cross-section assumed in the model (κ_X=2.22, δ_X=0.58, ψ^+=18°, ψ^-=68°).

Fig. 2. Ignition curves for the ITER reference parameters [Eqs. (65-67)], and f_L=1.84, 1.93, 2.0; Troyon beta limit curve (g=3); Greenwald density limit, and constant fusion power curve P_{fus}=1100 MW.

Fig. 3. Effect of the density peaking parameter on the minimum value of f_L required for ignition with P_{fus}=1100 MW in the ITER reference machine and corresponding optimum ignition temperature. Dotted line is from analytical expression Eq. (51).

Fig. 4. Effect of the temperature peaking parameter on the minimum value of f_L required for ignition with P_{fus}=1100 MW in the ITER reference machine and corresponding optimum ignition temperature. Dotted line is from analytical expression Eq. (51).

Fig. 5. Effect of the fraction of ^{4}He on the minimum value of f_L required for ignition with P_{fus}=1100 MW in the ITER reference machine (Z_{eff}=1.7) and corresponding optimum ignition temperature. Dotted line is from analytical expression Eq. (51).

Fig. 6. Effect of the variation of Z_{eff} on the minimum value of f_L required for ignition with P_{fus}=1100 MW in the ITER reference machine (f_α=10%) and corresponding optimum ignition temperature. Dotted line is from analytical expression Eq. (51).

Fig. 7. Effect of the variation of T_e/T_i on the minimum value of f_L required for ignition with P_{fus}=1100 MW in the ITER reference machine and corresponding optimum ignition temperature. Dotted line is from analytical expression Eq. (51).

Fig. 8. Effect of the hypothesis on the value of the degrading power on the minimum value of f_L required for ignition with P_{fus}=1100 MW in the ITER reference machine and corresponding optimum ignition temperature. Dotted line is from analytical expression Eq. (51).

Fig. 9. Values of f_L for ignition with imposed values of $B_{tmax} \simeq 10.7$ T, $d_{BS} \simeq 1.13$ m, $q_\psi \simeq 3.06$, $\Gamma_n \simeq 1.09$ MW/m², and P_{fus} as a function as the torus aspect ratio, for P_{fus} = 1100, 1700, 2200, and 3500 MW. Dashed lines are from analytical expression Eq. (61).

Fig. 10. Values of f_L for ignition with Goldston scaling with imposed values of $B_{tmax} \simeq 10.7$ T, $d_{BS} \simeq 1.13$ m, $q_\psi \simeq 3.06$, $\Gamma_n \simeq 1.09$ MW/m², and P_{fus} as

a function as the torus aspect ratio, for P_{fus} = 1100, 1700, 2200, and 3500 MW. Dashed lines are from analytical expression Eq. (D.10).

Fig. 11. Ignition curves for the A=4, 1700 MW ITER-like tokamak with f_L=1.48, 1.52, 1.55 corresponding to contact with P_{fus}=3000, 1700, 1100 MW; Troyon beta limit curve (g=3); Greenwald density limit.

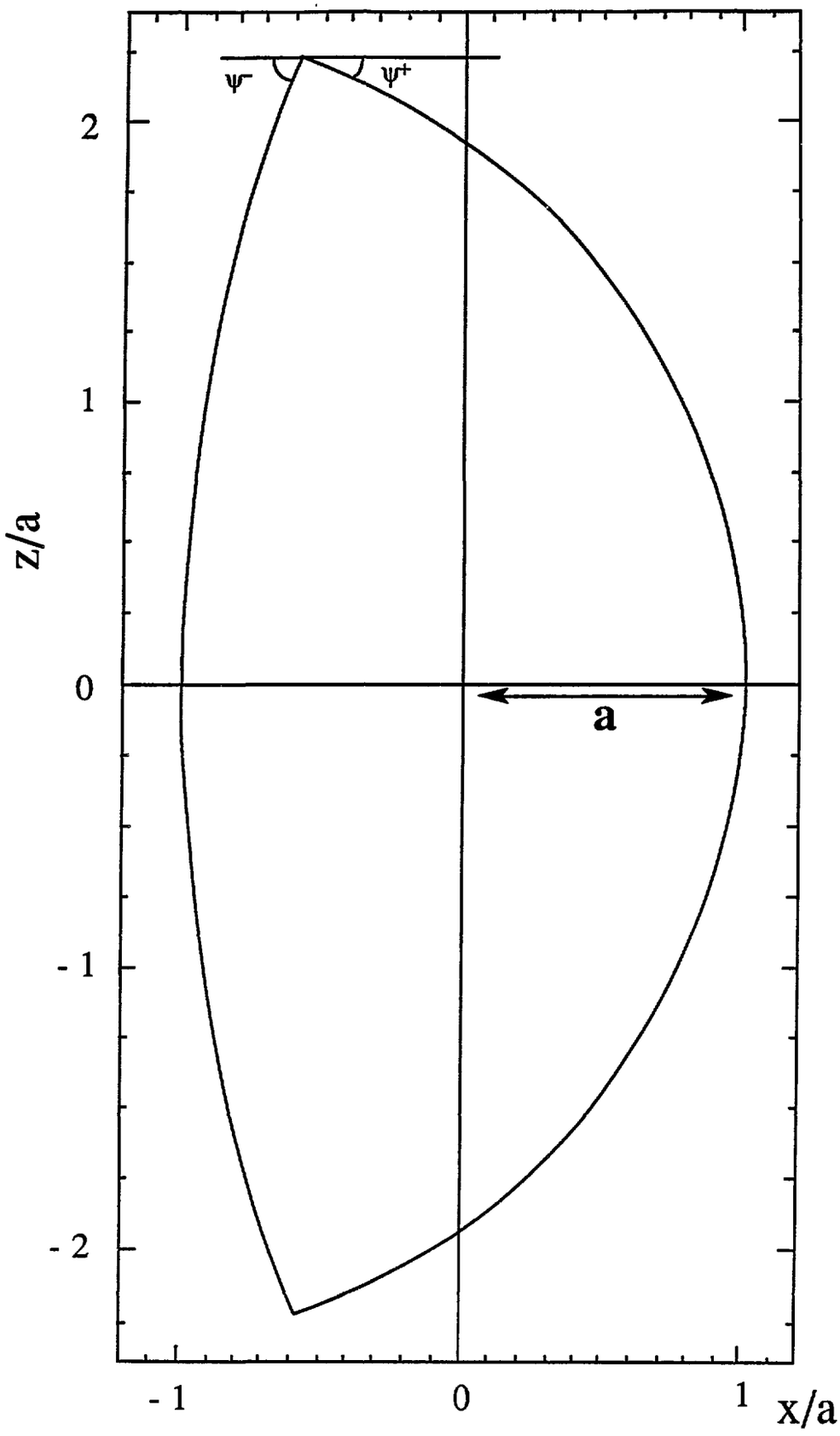

Fig. 1 : ITER plasma poloidal cross-section assumed in the model
($\kappa_x = 2.22$, $\delta_x = 0.58$, $\psi^- = 18°$, $\psi^+ = 68°$)

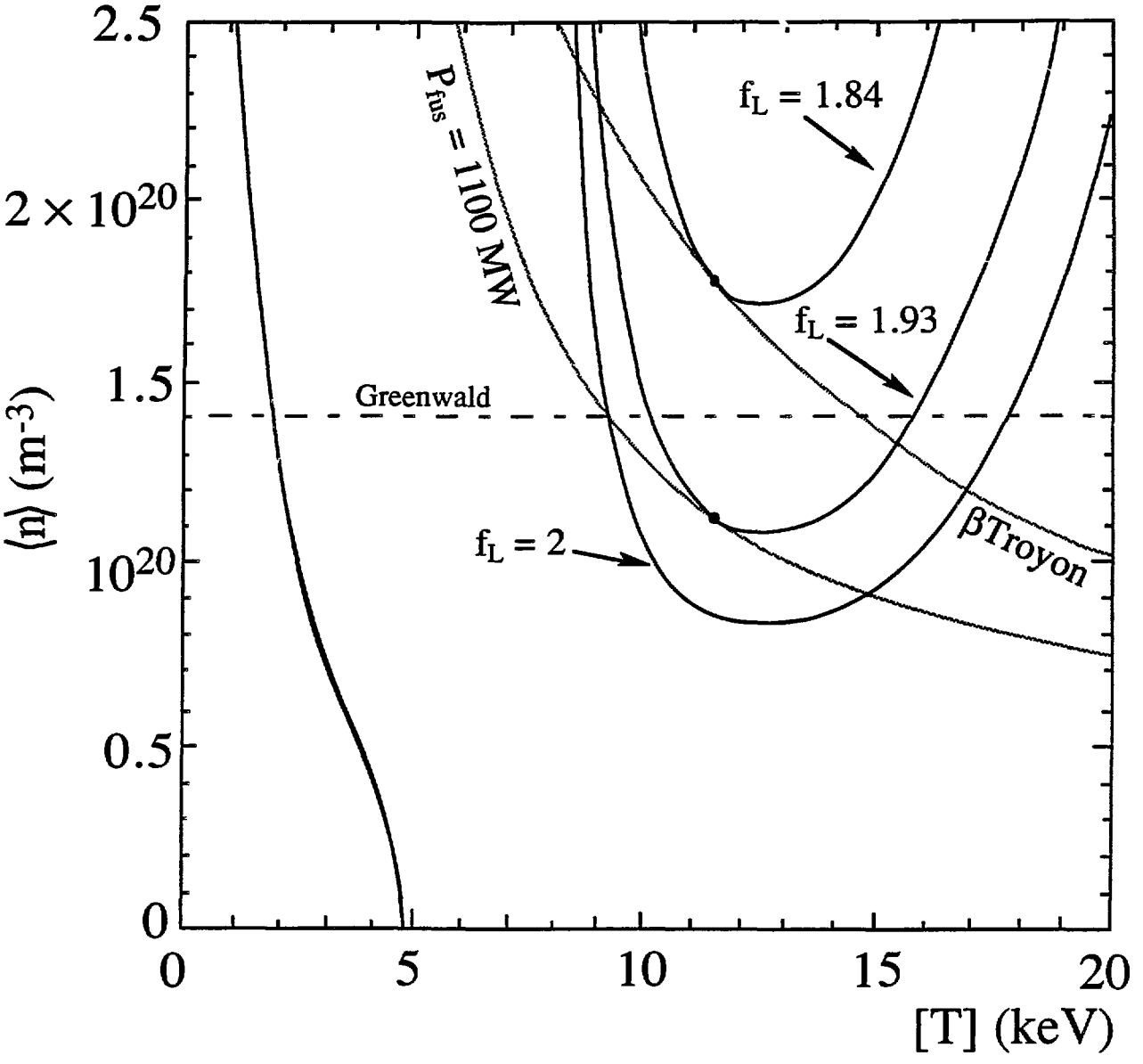

Fig. 2 : Ignition curves for the ITER reference parameters [Eqs. (65-67)] and f_L = 1.84, 1.93, 2 ; Troyon beta limit curve (g = 3) ; Greenwald density limit, and constant fusion power curve (P_{fus} = 1100 MW).

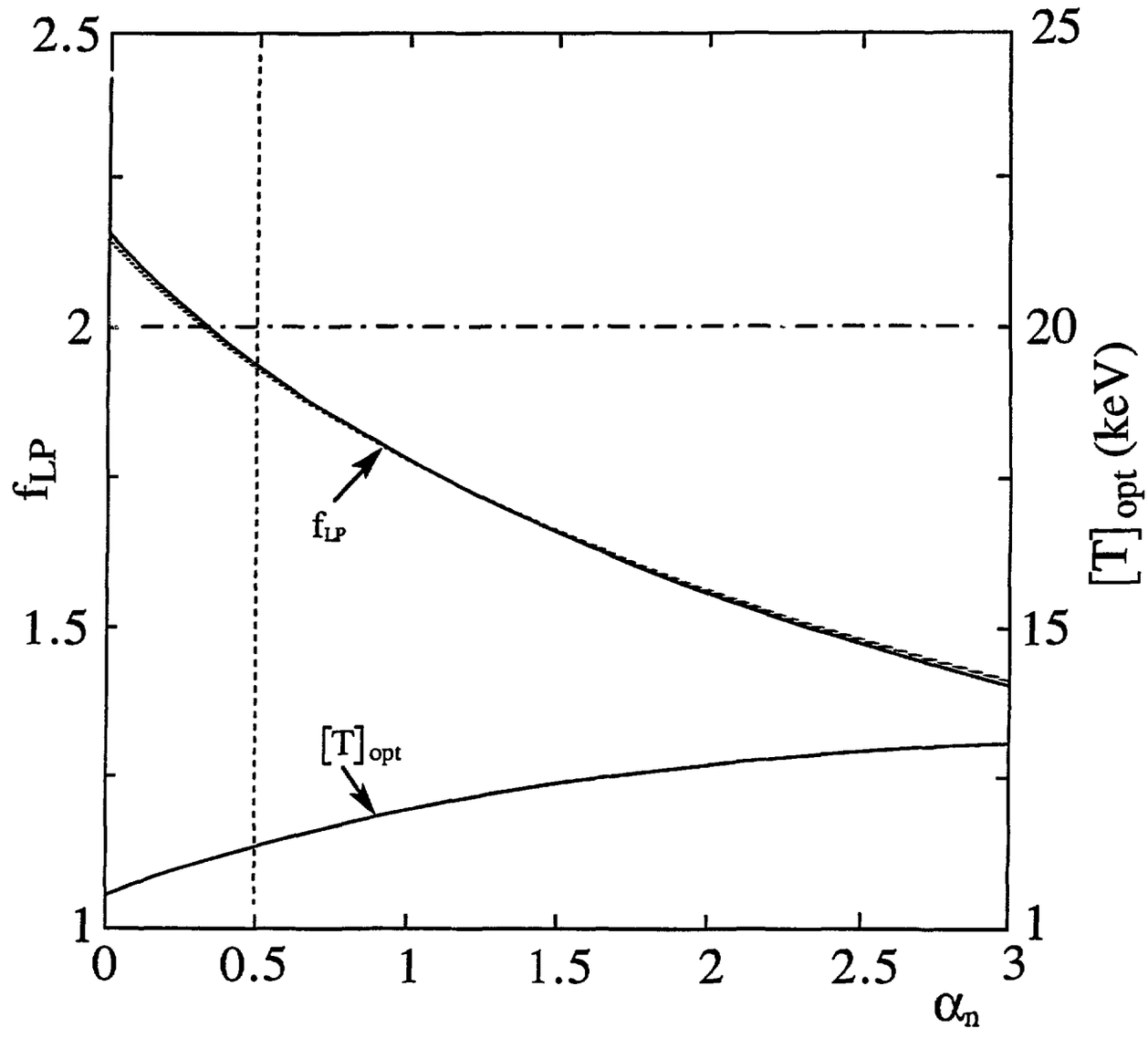

Fig. 3 : Effect of the density peaking parameter on the minimum value of f_L required for ignition with P_{fus} = 1100 MW in the ITER reference machine and corresponding optimum ignition temperature. Dotted line is from analytical expression Eq. (51).

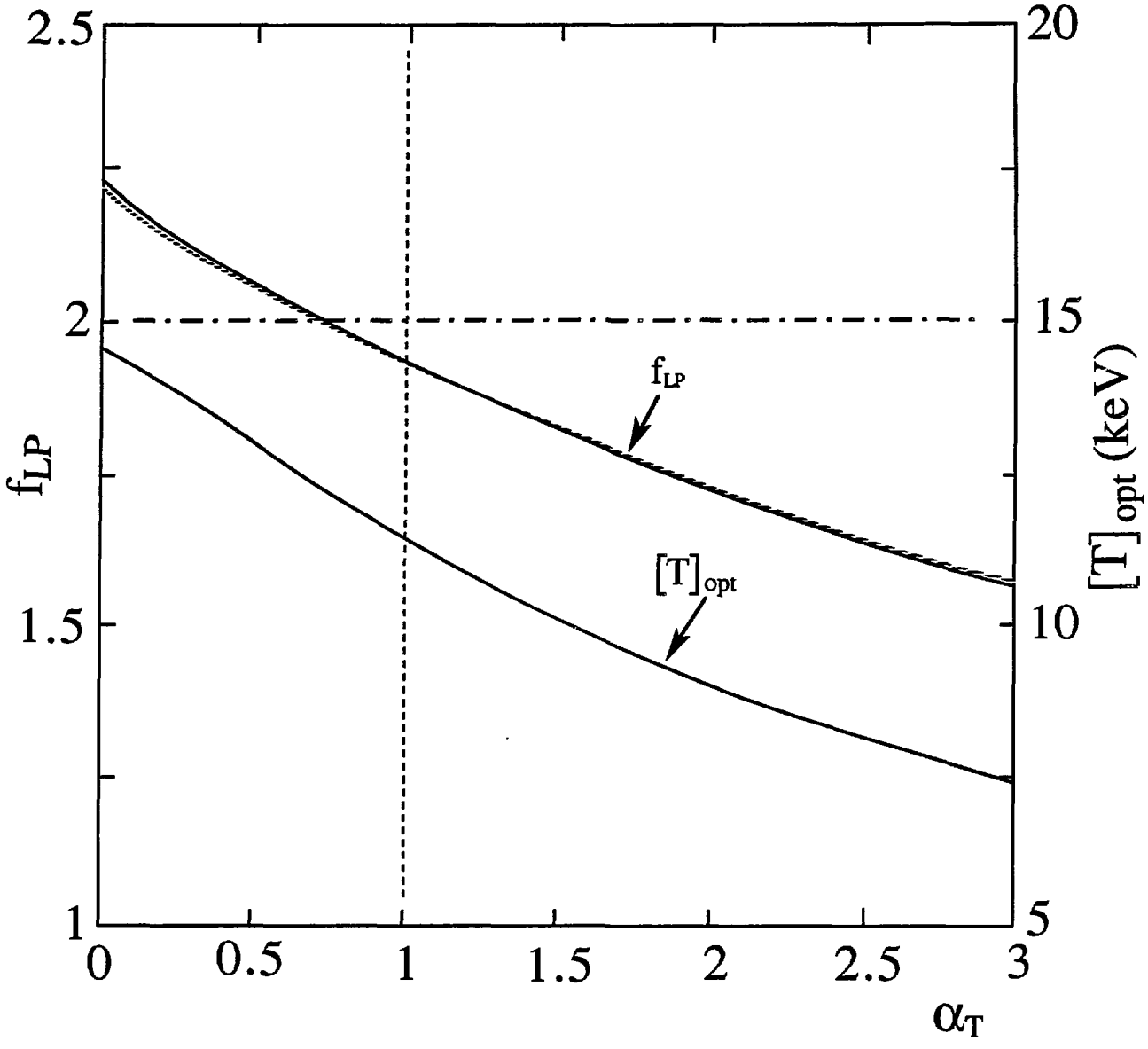

Fig. 4 : Effect of the temperature peaking parameter on the minimum value of f_L required for ignition with P_{fus} = 1100 MW in the ITER reference machine and corresponding optimum ignition temperature. Dotted line is from analytical expression Eq. (51).

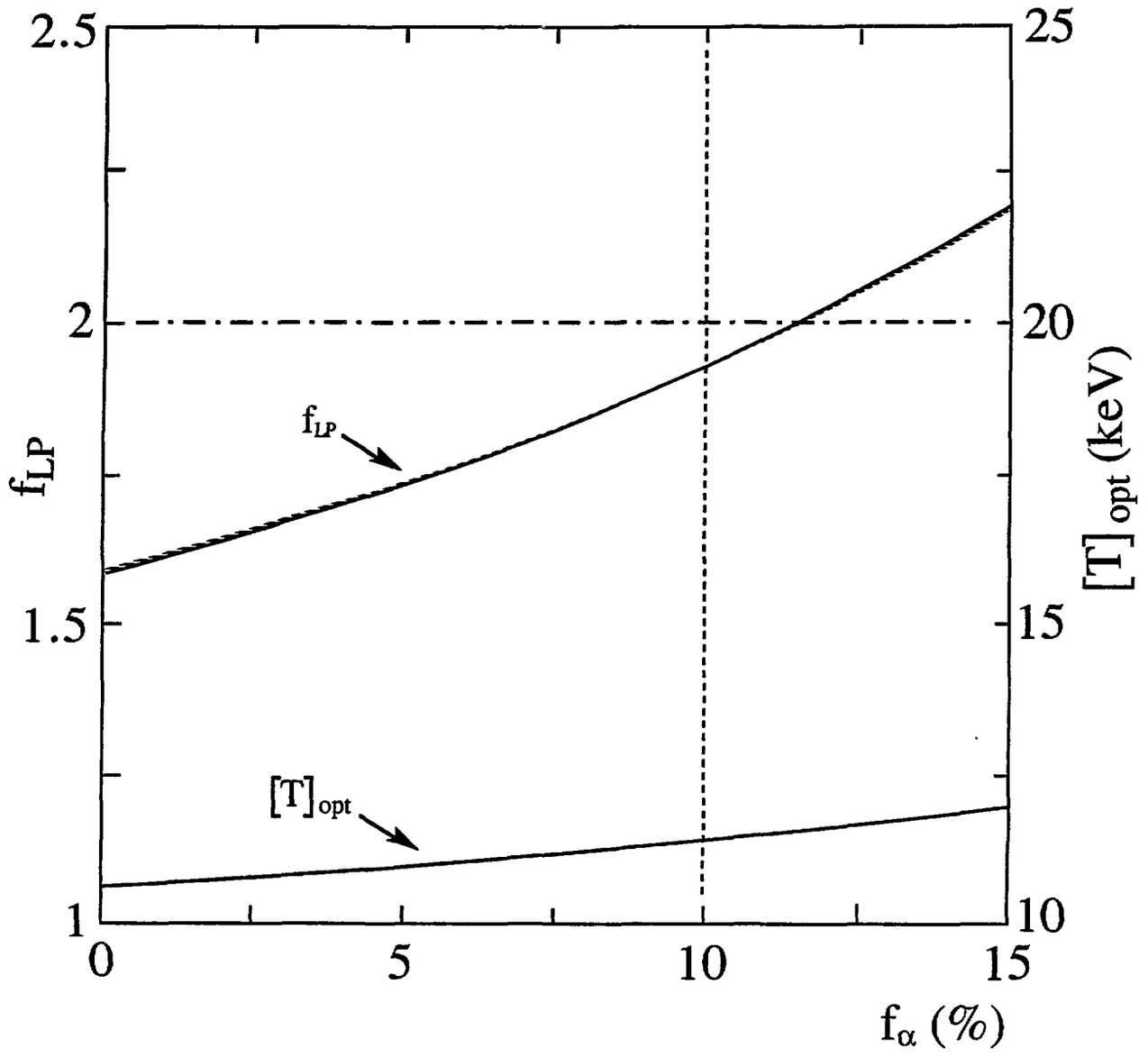

Fig. 5 : Effect of the fraction of ^4He on the minimal value of f_L required for ignition with P_{fus} = 1100 MW in the ITER reference machine (Z_{eff} = 1.7) and corresponding optimum ignition temperature. Dotted line is from analytical expression Eq. (51).

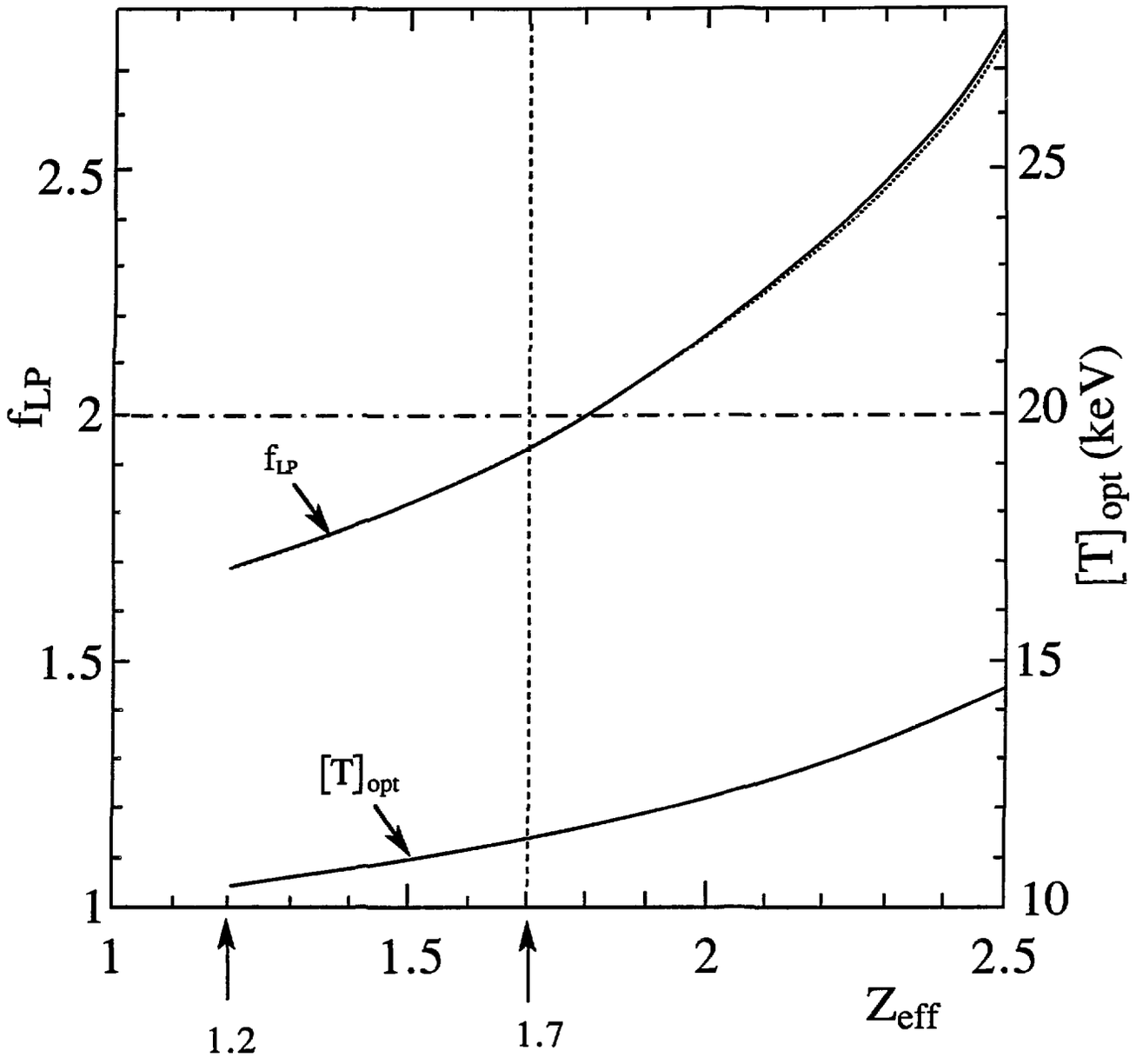

Fig. 6 : Effect of the variation of value of Z_{eff} on the minimal value of f_L required for ignition with P_{fus} = 1100 MW in the ITER reference machine (f_α = 10 %) and corresponding optimum ignition temperature. Dotted line is from analytical expression Eq. (51).

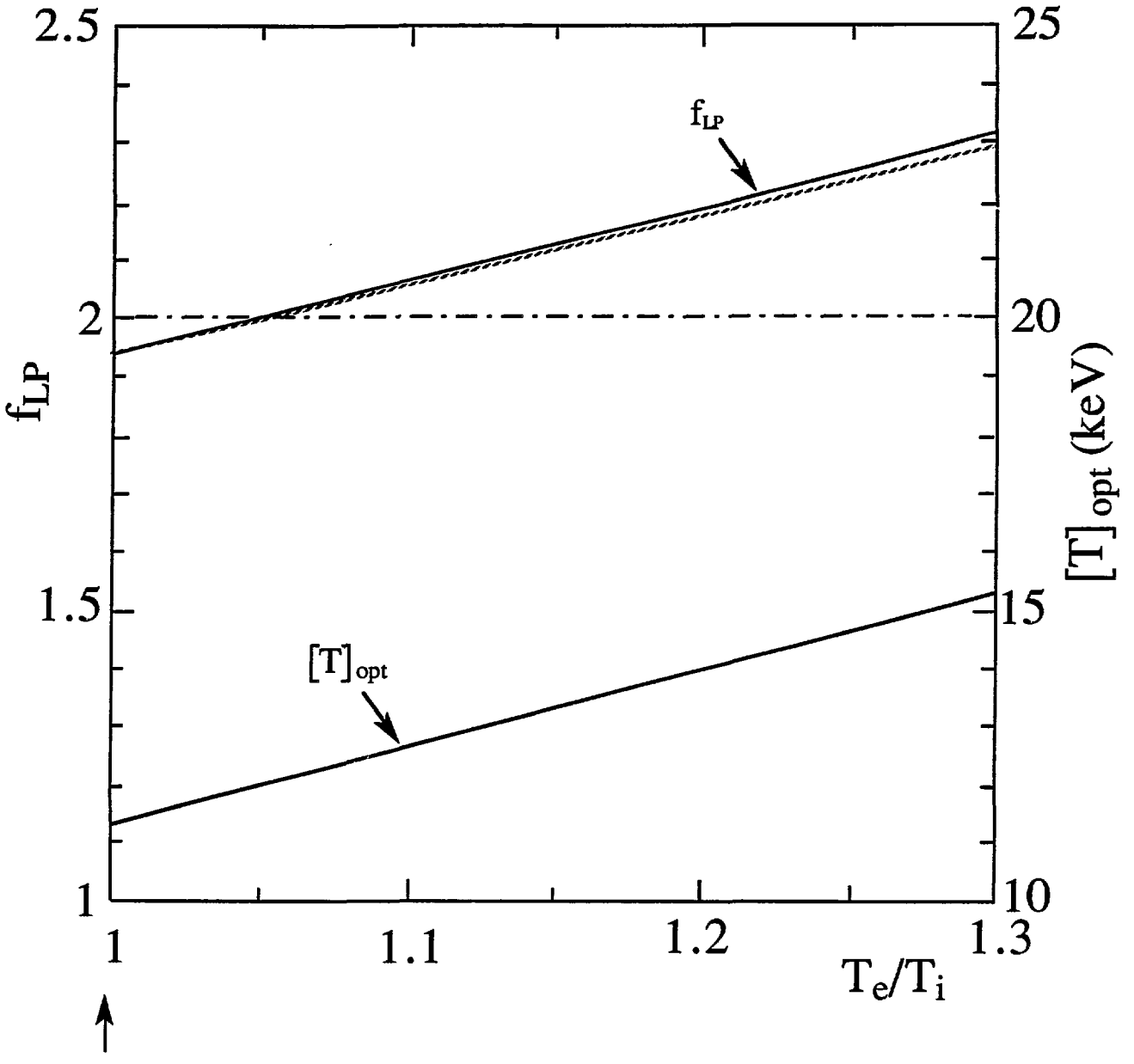

Fig. 7 : Effect of the variation of T_e/T_i on the minimal value of f_L required for ignition with P_{fus} = 1100 MW in the ITER reference machine and corresponding optimum electron temperature. Dotted line is from analytical expression Eq. (51)

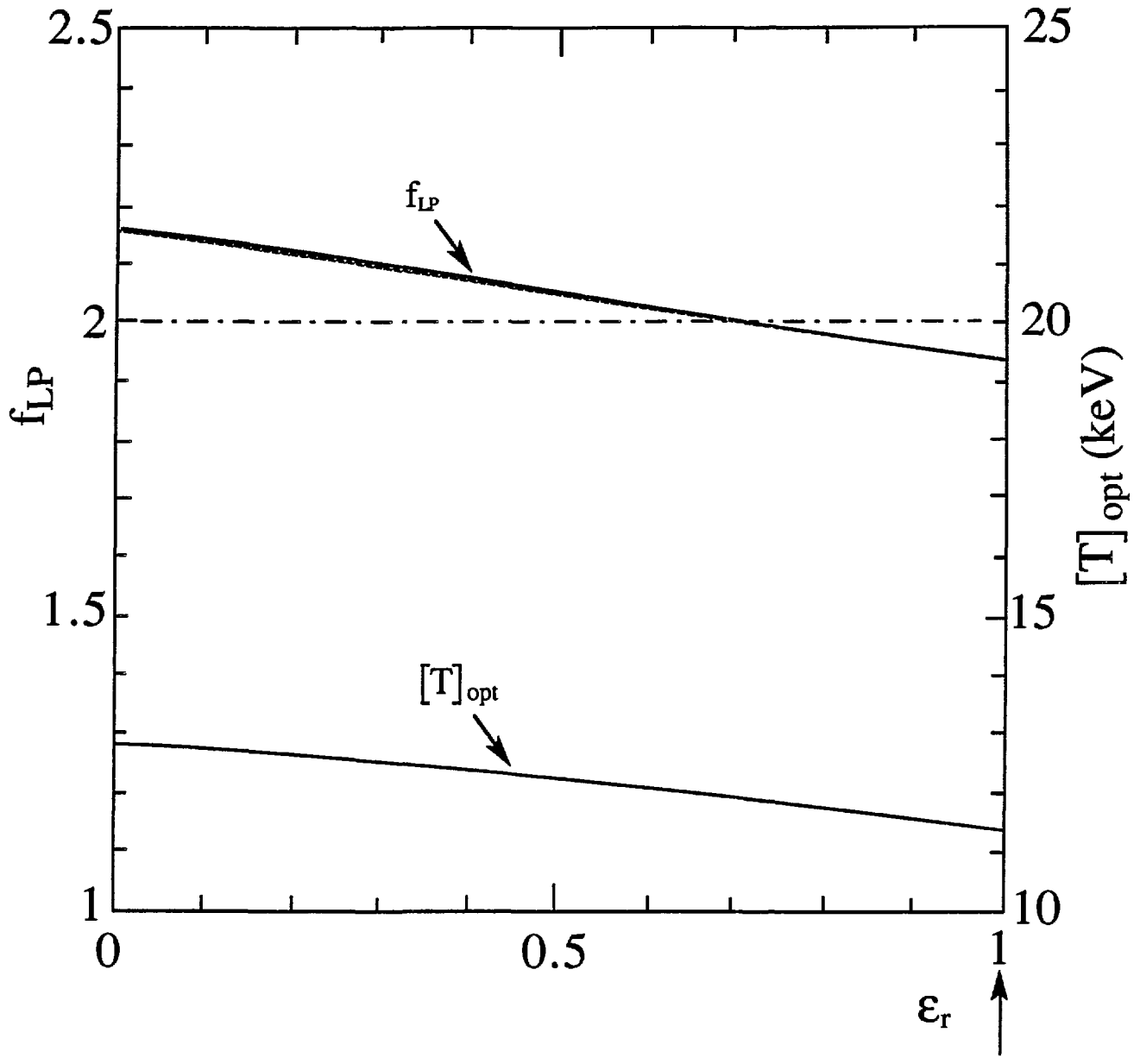

Fig. 8 : Effect of the hypothesis on the value of the degrading power on the minimum value of f_L required for ignition with P_{fus}= 1100 MW in the ITER reference machine and corresponding optimum electron temperature. Dotted line is from analytical expression Eq. (51).

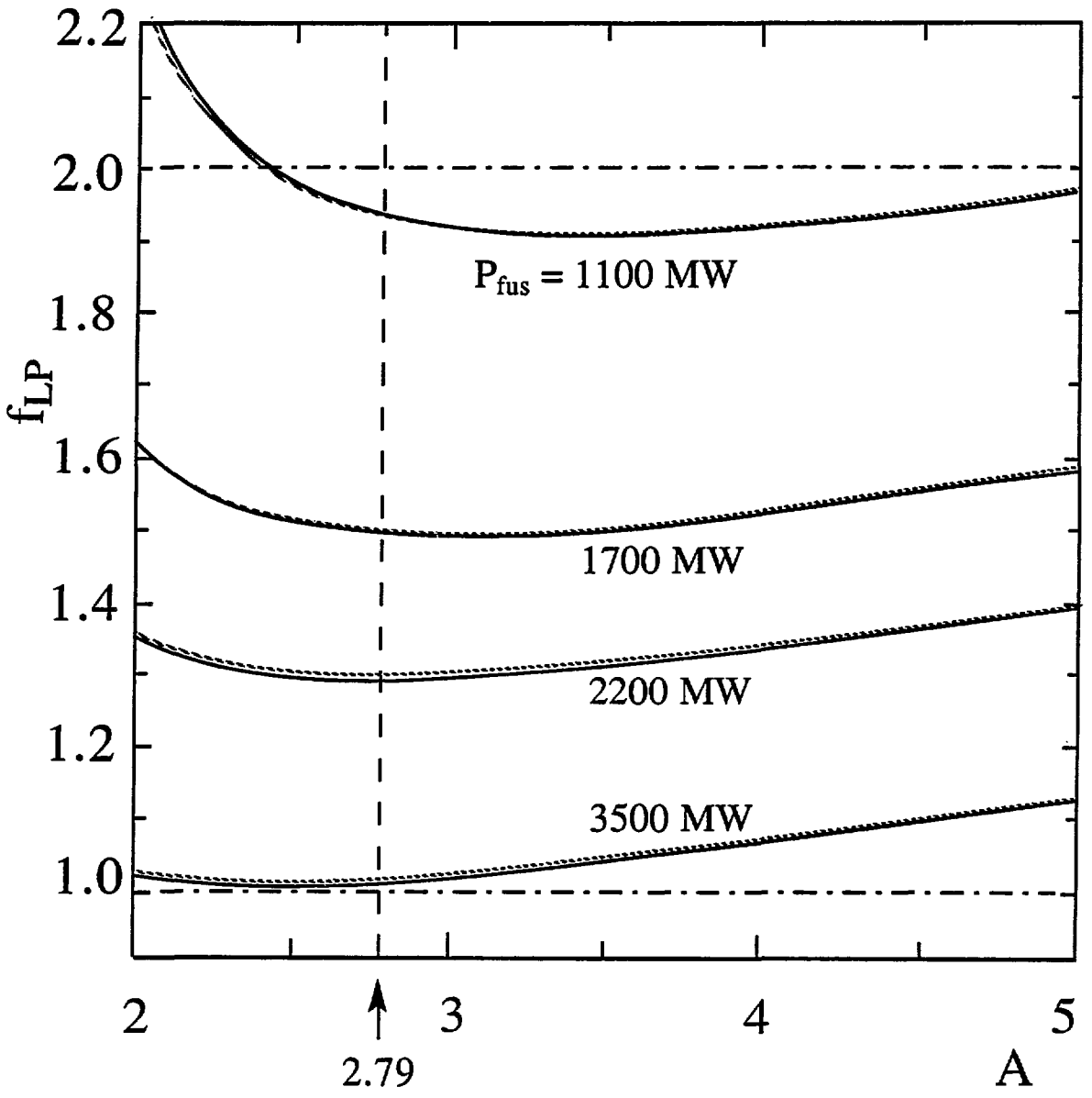

Fig. 9 : Values of f_L for ignition with imposed values of $B_{tmax} \approx 10.7$ T , $d_{BS} \approx 1.13$ m , $q_\psi \approx 3.06$, $\Gamma_n \approx 1.09$ MW/m^2 , and P_{fus} as a function of the torus aspect ratio, for P_{fus} = 1100, 1700, 2200, and 3500 MW. Dashed lines are from analytical expression Eq. (61).

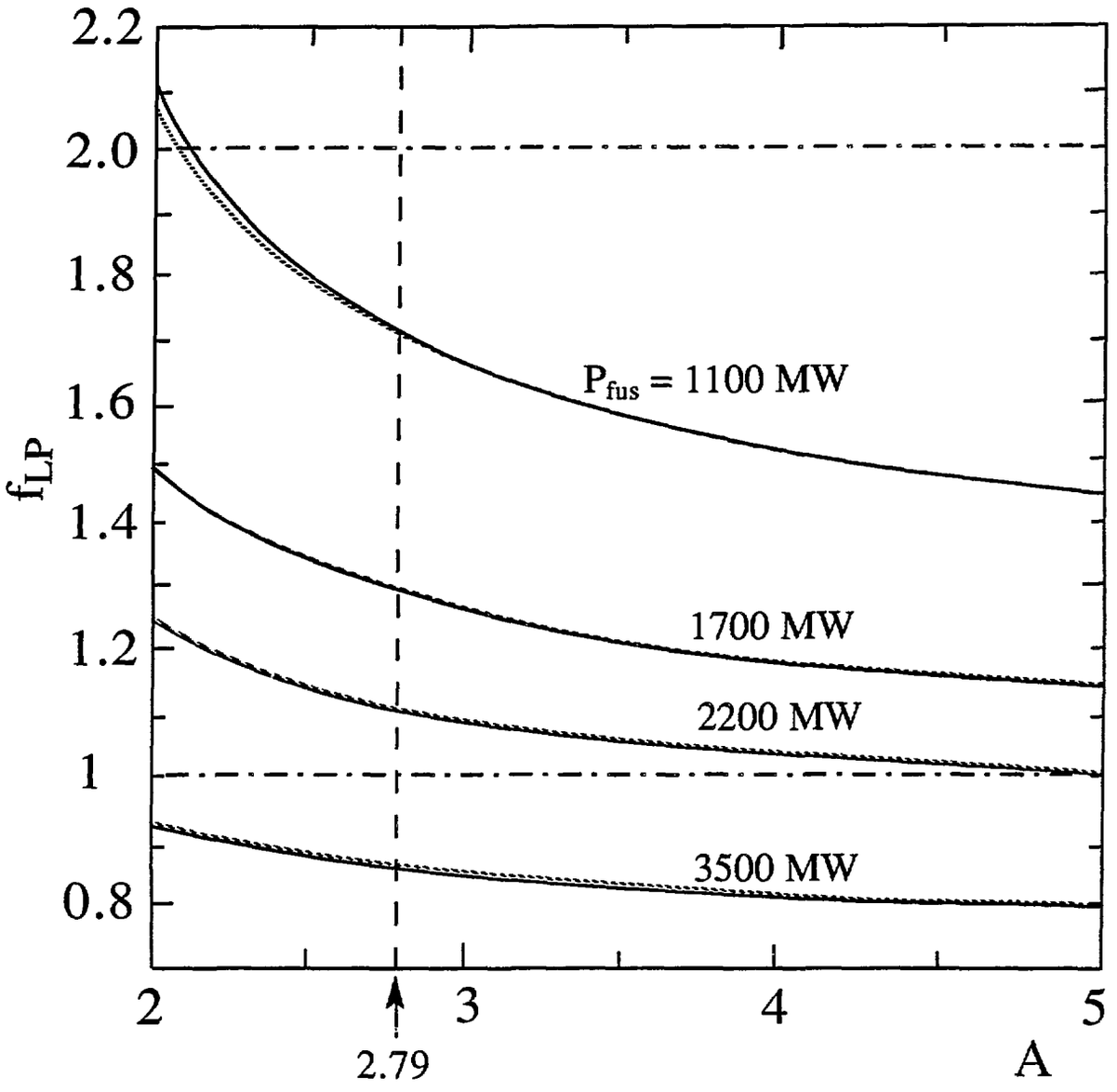

Fig. 10 : Values of f_L for ignition with Goldston scaling with imposed values of $B_{tmax} \approx 10.7$ T , $d_{BS} \approx 1.13$ m , $q_\psi \approx 3.06$, $\Gamma_n \approx 1.09$ MW/m^2, and P_{fus} as a function of the torus aspect ratio, for P_{fus} = 1100, 1700, 2200, and 3500 MW. Dashed lines are from analytical expression Eq. (D.10).

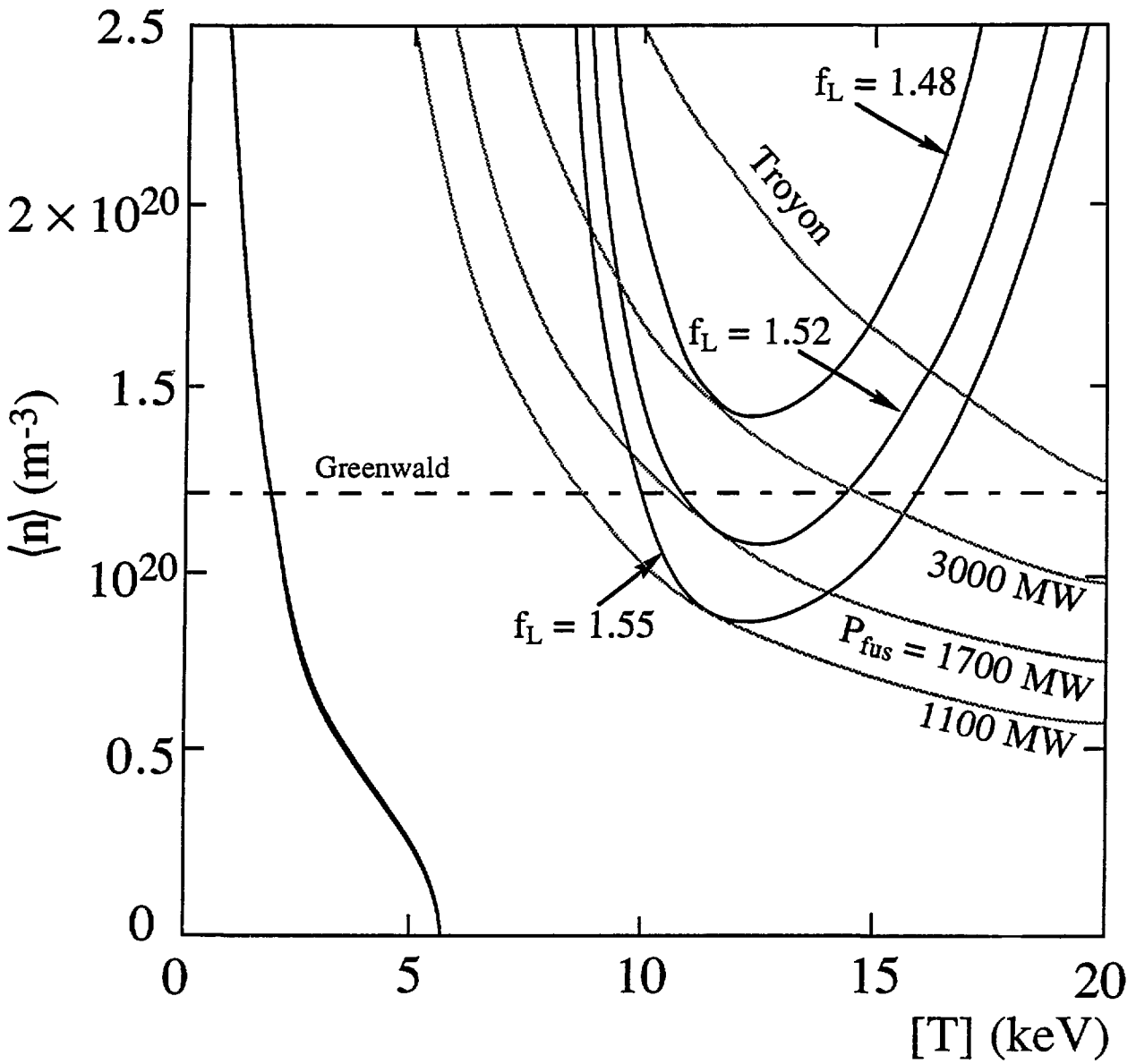

Fig. 11 : Ignition curves for the A = 4, 1700 MW ITER-like tokamak with f_L = 1.48, 1.52, 1.55 corresponding to contact with P_{fus} = 3000, 1700, 1100 MW ; Troyon beta limit curve (g = 3) ; Greenwald density limit.